The University of Sydney

Department of Civil Engineering
Sydney NSW 2006
AUSTRALIA

http://www.civil.usyd.edu.au/

Centre for Advanced Structural Engineering

Bending Tests of Bolted End Plate Connections in Cold Formed Rectangular Hollow Sections

Research Report No R736

Andrew T Wheeler BE
Murray J Clarke BSc BE PhD
Gregory J Hancock BSc BE PhD

January 1997

Copyright Notice

Department of Civil Engineering, Research Report R736
Bending Tests of Bolted End Plate Connections in Cold Formed Rectangular Hollow Sections

A.Wheeler@civil.usyd.edu.au, M.Clarke@civil.usyd.edu.au
G.Hancock@civil.usyd.edu.au

Published by:
Department of Civil Engineering
The University of Sydney
Sydney NSW 2006
AUSTRALIA

January 1997

http://www.civil.usyd.edu.au

Bending Tests of Bolted End Plate Connections in Cold Formed Rectangular Hollow Sections

A. T. Wheeler, B.E.
M. J. Clarke, B.Sc., B.E., Ph.D.
G. J. Hancock, B.Sc., B.E., Ph.D.

January 1997

Centre for Advanced Structural Engineering
School of Civil and Mining Engineering
University of Sydney, N. S. W., Australia, 2006

Abstract

The research report describes an experimental investigation into the flexural behaviour of bolted end plate connections joining cold formed square and rectangular hollow sections. A total of twenty six (26) specimens, joined at midspan using a bolted end plate connection then loaded under four point bending, were tested in a servo-controlled testing machine. The primary aim of the investigation was to evaluate the effect of various end plate parameters on the connection strength and serviceability. The results of the bending tests are tabulated in the report, and graphs detailing the behaviour of each specimen are also presented. The experimental data will facilitate the development and verification of design models for the bolted moment end plate connection joining rectangular section tubes, and will provide data on the non-linear moment rotation characteristics of the connection.

TABLE OF CONTENTS

1. Introduction

For both aesthetic and economic reasons, the use of tubular members in steel building frames has increased in recent years. Aside from their use in prominent architectural structures, tubular members are increasingly becoming a feature of more "mainstream" steel structures such as industrial portal frames and multistorey steel frames. The economics of prefabrication mean that the connections in these frames are moving from traditional welded connections, as found in trusses and off-shore structures, to bolted connections that are prefabricated, transported and then assembled on site.

The bolted end plate connection discussed in this report is one such connection which can be fabricated and erected easily, providing an economical tubular connection. While used extensively as a shear connection, this connection may also be used as a moment connection, and can be designed to achieve a high degree of rotational stiffness. In addition, with the ever-present drive for more economic structures, and the advent of more powerful computer analysis programs, an interest in assessing and utilising the resistance provided by semi-rigid connections has emerged. This is recognised in the current Australian Limit States Standard for Steel Structures (SA ,1990) which allows for the design of semi-rigid connections within a structure "if the relationship between the degree of flexural restraint and the level of load effects has been established by methods based on test results".

The moment end plate connection joining I-section members has been used extensively, and considerable documentation on its behaviour exists in the literature (for example, Grundy et al., 1980; Kukreti et al., 1990). By contrast, research on end plate connections joining rectangular and square hollow sections has been limited, and furthermore has concentrated primarily upon pure tensile loading (Kato and Hirose, 1985; Packer et al., 1989), or combined compression and bending (Kato and Mukai, 1991) as in a column-to-column bolted flange splice connection.

Moment end plate connections of the nature studied in this report have several possible applications in tubular structures, some of which are shown in Figure 1. The connection depicted in Figure 1a is a moment resisting beam splice connection, and this is actually the configuration employed herein for experimental investigative purposes. A column base plate connection of the type shown in Figure 1b is another application of the moment end plate connection addressed in this report. A third application,

illustrated in Figure 1c, shows a possible means through which the end plate connection can be used as a moment resisting beam-column connection.

This report presents the results of tests on bolted moment end plate connections joining square and rectangular hollow sections subjected to pure flexure. The parameters that were varied in the tests are: (1) the thickness of the end plate; (2) the number of bolts in the connection; (3) the proximity of the bolts to the section perimeter; (4) the width of the end plate; and, (5) the shape of the section (i.e., square or rectangular). The presented results include the ultimate moment capacity of the connections and the moment-rotation relationship for each test.

2. Connection Classification Schemes

In the elastic or inelastic analysis of frames for design, it is ideal to consider the effect of the connection behaviour on the overall frame response. For convenience, it is common practice to classify and to model these connections as either perfectly pinned or fully rigid, although most connections fall between these extremes. For example, shear connections, which are nominally pinned, invariably have a finite moment capacity. While moment connections of the type reported herein may be considered rigid, it is possible that their flexural strength is lower than that of the corresponding beam.

The behaviour of a connection can be defined in terms of its moment-rotation curve, which may be obtained either through theoretical procedures or experimental research. This behaviour is often highly non-linear, and it is often inappropriate to classify the connection as either rigid or pinned. To aid in the design and analysis of connections, several classification schemes based on the total moment-rotation behaviour have been developed.

It should be borne in mind that the classification of any connection as flexible, semi-rigid or rigid is not absolute as the rotational stiffness of the connection varies with the applied moment. For example, a particular connection with a high initial stiffness and low design moment may be justifiably assumed to be “rigid”. However, the same connection acted on by a much greater design moment (approaching the connection ultimate strength, say) may be more appropriately considered as “semi-rigid” for design purposes. The limiting moment for rigid design of a connection can be referred to as the “rigid limit” and defined by the point at which the transition from the “rigid” zone to the “semi-rigid” zone occurs. Another shortcoming of connection classification schemes, as will be explained later, is that they are generally dependent on the member geometry.

Connection classification schemes attempt to characterise the connection using the full range moment-rotation response as would ideally be employed in non-linear inelastic (advanced) frame analysis. One of the aims of this report is to classify the moment end plate connections as "semi-rigid" or "rigid", and to this end the full-range response of the connection in conjunction with a recognised classification scheme (Bjorhovde *et al*., 1990) is employed.

Connection classification schemes which have been proposed include those of Bjorhovde *et al*. (1990) (see Figure 2) and Eurocode 3 (CEN, 1992). Both of these schemes classify connections into the following three basic categories according to the moment-rotation characteristic: (1) Flexible; (2) Rigid; and (3) Semi-rigid. The usual practice is to express the connection moment (M) and rotation (θ) in a non-dimensional form. The moment is non-dimensionalised using the expression $\overline{m} = M/M_p$ in which M_p is the plastic capacity of the connected beam section. The non-dimensionalised rotation parameter $\overline{\theta}$ is dependent on the classification scheme selected. The Eurocode 3 scheme uses the actual length L_b of the beam in the structural system to determine $\overline{\theta}$, defining $\overline{\theta} = \theta_c / (M_p L_b / E I_b)$ in which θ_c is the connection rotation. The Bjorhovde *et al*. (1990) scheme uses a reference length of five times the beam depth to define the connection rotation parameter $\overline{\theta} = \theta_c / (5 M_p d / E I_b)$. The use of the beam depth, d, by Bjorhovde has the advantage that it can be used by the designer to classify connections prior to the determination of any beam lengths L_b. For this reason the Bjorhovde scheme will be used in this report for connection classification purposes.

The Bjorhovde classification scheme, shown in Figure 2, classifies connections in terms of their *strength* and *stiffness*. For stiffness, the semi-rigid connections are defined as those with an initial stiffness $\overline{m}/\overline{\theta}$ in the range of 0.5 to 2.5. In terms of strength, a semi-rigid connection is identified as having an ultimate strength defined by $\overline{m}$ greater than 0.2 but less than 0.7. Connections falling above or below these limits would be classified as rigid or flexible, respectively. In the classification of a connection, the rotation θ_c used is the rotation of the connection relative to the attached beam (see Figure 3), while M_p, d and EI_b are the plastic moment capacity, depth and flexural rigidity, respectively, of the beam section.

3. Test Specimens and Properties

3.1 Specimen Details and Fabrication

This investigation examined the behaviour of bolted moment end plate connections in cold-formed rectangular hollow sections (RHS) and square hollow sections (SHS). To eliminate the possibility of the connection strength being limited by local failures within the beam, compact sections (sections with *b/t* ratio of less than 16) were selected. The nominal section sizes are shown in Table 1, and further details on the sections can be found in the Design Capacity Tables for Structural Steel Hollow Sections (AISC, 1992). The nominal yield stress of the tubular section is 350 MPa. The sections were manufactured to the requirements of AS 1163 (SA, 1991a).

A total of twenty six (26) connection tests were performed. The tests were divided into two series: Type A connections (Tests #1-10) which consisted of eight bolts; and the Type B connections (tests #11-26) which contained four bolts. In both series, rectangular and square hollow sections were tested.

An additional three (3) tests were carried out on beam sections to determine the comparative beam behaviour without the inclusion of the connection. Two full beam tests were conducted (one RHS and one SHS) to determine the bending behaviour of the sections. To establish the effect of the weld on the behaviour of the section a third test was performed on a beam cut at midspan, then prepared and welded in an identical manner to the connections (but without a bolted end plate).

3.1.1 End Plate Details

The general layout of the end plates is shown in Figures 4a and 4b for Type A and Type B connections, respectively, with the thickness (t_p) and dimensions (W_p, D_p) of the plates detailed in Table 2. The distance from the edge of the plate to the centre of the bolts (a_e) was constant for all tests and set at 30 mm according to the edge distance limits specified in AS 4100 (SA, 1990).

In test series Type A, two parameters were varied: the thickness of the end plate (t_p), and the distance from the perimeter of the tubular section to the bolts (s_o). The plate width (W_p) and plate depth (D_p) are dependent on the bolt position (s_o), and are shown in Table 2. The pitch of the bolts is defined by the variable *g*, the distance from line of the webs to the bolt holes, and was chosen such that the spacing, in a circumferential sense, of the eight bolts is approximately equal.

In test series Type B, the end plate thickness (t_p) was again varied. The distance from the flange of the section to the bolt (s_o), and the distance from the web to the horizontal position of the bolts (c) were also varied. The plate width (W_p) is dependent upon the bolt position (c), while the plate depth (D_p) is dependent upon the bolt position (s_o).

All holes were clearance holes (diameter 22 mm) for M20 bolts. The end plate material was 350 grade steel, to AS 3678 (SA, 1981b) with a nominal yield stress of 350 MPa.

3.1.2 Bolt Details

In all but four tests (#13, #13*, #19 and #19*) the bolt assemblies used in the connections were ungalvanized M20 high strength structural grade nuts and bolts (grade 8.8/T). Tests #13 and #19 utilised corresponding galvanized bolt assemblies from the same manufacturer (Ajax Fasteners, 1992), since the ungalvanized bolts used in the previous tests are no longer available. Tests #13* and #19* were performed using ungalvanized M20 “metric” grade 8.8 bolts from an alternative manufacturer.

All the bolts are manufactured to the requirements of AS 1252 (SA, 1981a), with a nominal proof stress of 840 MPa. The length of bolt (l_B) used for each test depended on the end plate thickness, and details are given in Table 2. Further details on these bolt assemblies can be found in the manufacturer’s catalogue (Ajax Fasteners, 1992).

3.1.3 Fabrication of Specimens

A typical layout of a test specimen is shown in Figure 5. The sections were orientated in such a manner that the electric resistance weld in the tube was always positioned in the web of the specimen. To avoid any problems of bearing failure at the points of load application and the support points, plates 150 mm wide and 10 mm thick were welded to both webs of the section. These plates protruded below the section at the support end and above the section at the loading points, and facilitated the introduction of loads directly into the webs of the section.

The end plates were welded with a combination butt/fillet weld to the ends of the sections. As these welds were specified as an SP Category weld, pre-qualification of the welding procedure was carried out in accordance with AS 1554.1 (SA, 1991c). The weld preparation and procedure together with the relevant qualifying tests are given in Appendix B.

3.2 Material Properties

3.2.1 End Plate Tensile Coupons

Tensile coupons were taken from each of the three end plate thicknesses, then prepared and tested in accordance with AS 1391 (SA, 1991b) to determine the yield stress (f_y) and tensile strength (f_u).

3.2.2 Section Tensile Coupons

Three tensile coupons were taken from most hollow sections, the first from a corner of the section, the second from the flange of the section, and the third from the web face not containing the seam weld. The coupons were prepared and tested in accordance with AS 1391 (SA, 1991b) to determine the yield stress (f_y), the tensile strength (f_u), and the percentage elongation (e_u) at the ultimate strength. To enable testing of the corner coupons in the same manner as the flat coupons, their ends were pressed flat.

3.2.3 Coupon Testing

The majority of the tensile coupon tests were performed in a 250 kN capacity Instron Universal Testing machine, with a 2000 kN Dartec testing machine being used for the 20 mm end plate coupons. All coupons had a pair of 20 mm strain gauges placed on opposite faces to measure the strain. A displacement transducer was also placed on the crosshead of the testing machine to measure the induced elongation. The specimens were placed in the appropriate testing machine and loaded using displacement control at a rate of 0.05 cm/min. The longitudinal displacement and the applied load were plotted continuously, and readings of these parameters and the strain were recorded periodically using a Spectra data acquisition unit. By observing the load displacement plot, the yield load could be identified and the crosshead halted. By holding this displacement for two minutes the 'zero strain rate' yield stress (f_y) value was determined. This procedure was repeated in the vicinity of the ultimate load to determine the ultimate tensile strength (f_u).

The measured values of yield stress (f_y), ultimate tensile strength (f_u) and the percentage elongation at ultimate (e_u) are presented in Table 3 and Table 4 for the hollow sections and the end plate, respectively. Typical stress-strain curves for the section coupons and the plate coupons are shown in Figures 6 to 8. For the test pieces that exhibited no yield plateau, the yield stress f_y is taken as the 0.2 percent proof stress as shown in Figure 6. The elongation at ultimate (e_u) was measured at the point immediately preceding the shedding of the load. The average measured values of f_y and f_u are compared with their respective nominal values from AS 1163 (SA, 1991a) (f_{yn} = 350 MPa and

f_{un} = 430 MPa for the section), and from AS 3678 (SA, 1981b) (f_{yn} = 350 MPa and f_{un} = 450 MPa for the end plate). For the sections, the ratio f_y/f_{yn} ranged from 1.08 to 1.43 and the value of f_u/f_{un} was between 0.96 and 1.22, while for the end plate the ratio f_y/f_{yn} ranged from 1.00 to 1.01 and the ratio f_u/f_{un} was between 1.07 and 1.11. The percentage elongation experienced in the section corners was much lower than for the section flats, this being due to the greater cold work done on the section corners during manufacture. For the plate material, values of e_u in excess of 20 % were obtained.

An estimate using the initial elastic portion of the stress-strain curve was used to determine the elastic modulus (E) for the sections. An average value of E = 205000 MPa was determined for the flats of the cold formed sections, while an average value of E = 208000 MPa was determined for the corners of the cold formed sections. The plate material demonstrated an ideal elastic plastic behaviour with an average value of E = 207000 MPa being ascertained for this material.

3.2.4 Bolt Tensile Properties

The tensile properties of the M20 bolts were obtained by testing individual bolt and nut assemblies in a 2000 kN Dartec testing machine. Using a purpose built testing rig, the load was applied using displacement control at a slow rate to obtain the static tensile load of the assembly. The elastic modulus of the bolts was determined by testing a bolt containing a strain gauge mounted concentrically in the shank of the bolt. These strains were plotted against the applied load to obtain the load-strain relationship for the bolts, shown in Figure 9. The average ultimate load for the bolts was found to be 230 kN, with an elastic modulus of 209000 MPa.

4. Joint Testing Procedure

4.1 Test Set-up

A schematic view of the general test set-up, and a picture of a specimen being tested are shown in Figure 10 and Figure 11 respectively. Each test consisted of a pair of identical halves bolted together to form a beam specimen with the connection at mid-span. The support plates of the beam specimens were placed on half rounds which in turn were placed on Teflon pads. The bottom surface of the half rounds were machined to a high degree of smoothness to allow sliding on the Teflon pads. This sliding was further enhanced by lubrication of the interface between the half round and the Teflon pad, giving an idealised roller pin support. Due to the fact that high rotations were experienced by the beam specimens during testing, the loading points were similarly set up using inverted half rounds, with the

chord face of the half round facing upwards, and the lubricated Teflon pads and spreader beam placed on top as shown in Figure 10. This allowed the supports and loading points of the specimen to rotate and slide horizontally. This layout ensured the satisfactory modelling of the simply supported beam and avoided the introduction of a net tensile force into the specimen.

The simply supported beam specimens were tested by loading symmetrically at two points within the span using a spreader beam loaded centrally by the hydraulic ram. In this manner, the connections were tested in pure bending in the absence of shear, as shown by the bending moment and shear force diagrams in Figure 12. This method enabled the simple calculation of the moment applied to the connection, given that the initial lever arm (l), the distance from the support to the loading point, was 450 mm for all specimens.

4.2 Instrumentation

4.2.1 Rotation Measurements

An important quantity to measure is the rotation of the connection itself, which corresponds to the change in the slope of the tangents to the deflected shape across the connection. This rotation is denoted θ_c in Figure 3. Practical considerations within the experimental procedure, however, usually dictate that the rotation measurements are taken over a finite length of the beam. The corresponding rotation is termed θ_t in Figure 3. Thus the total rotation of the connection (θ_t) measured is the sum of the connection rotation (θ_c), and the rotation generated by the curvature of the beam section (θ_s) as shown in Figure 3.

The rotation θ_t is measured as shown in Figure 13 using two rods which are passed vertically through and fastened to the flanges of the beam section either side of the connection. The rods are positioned in the middle of the flange, and at a distance of l_r from the midpoint of the connection. Displacement transducers are positioned at the top of one rod and the bottom of the other rod (perpendicular to the rod), to measure the extensions and contractions between the ends of the two rods (Figure 13). From these measurements the total rotation of the connection (θ_t) can be calculated.

The rotation of the beam section (θ_s) was determined using the measured values of strain in the beam during the tests. These values were measured using strain gauges mounted on the centre of the top and bottom flanges of the section, at a distance equal to the depth of the section from the adjacent end plate. It is assumed that at this distance the longitudinal bending strains

are reasonably representative of engineering bending theory and are not greatly affected by the complex state of stress in the immediate vicinity of the connection. The rotation (θ_s) was calculated assuming the curvature is uniform over the length l_r.

4.2.2 Plate Separation

End plate separation at the tensile side of the connection is a parameter of great importance as it indicates a departure from full connection rigidity to the more flexible and non-linear connection behaviour. The plate separation also gives an indication of if, and when, a mechanism has formed in the end plates.

The end plate separation was measured at the toe of the weld on the bottom side of the connection. A pair of displacement transducers was mounted on the bottom flange running parallel with the section. The first transducer passed through the adjacent plate, by means of a small hole, and monitored the movement of the opposite plate. The second transducer monitored the movement of the adjacent plate. The real plate separation was then determined by calculating the difference between the measurements recorded by the first and second transducers (see Figure 13).

4.2.3 Bolt Loads

The bolts are a critical part of the connection and it was therefore important to monitor their behaviour during testing. Forces in the bolts were measured using a small 10 mm high cylindrical load cell placed under the head of each bolt. These load cells are detailed in Figure 14a. The yield stress of the load cells was 1280 MPa and the ultimate tensile strength was 1420 MPa. Three strain gauges were placed on the circumference of the load cell, to measure the induced loads. The finite size of these load cells resulted in an increase in the bolt grip of between 19% and 27% depending on the end plate thickness. This may have a minor effect on the connection ultimate strength, but has a significant effect on the stiffness of the connection. This effect was minimised by using load cells which were as short as practicable. The use of short load cells, however, compromised the accuracy of the bolt force measurements, with calibration studies indicating that the measured forces are only accurate to within about 15%. Although not able to measure the bolt forces with high reliability, the load cells were invaluable for providing insight into the quantitative behaviour of the bolt forces, and hence the connections, throughout the load history. For the two final tests (Tests #13 & #19), fully instrumented bolts (with strain gauges placed concentrically in the shank) were used in addition to the load cells, giving more accurate results.

4.2.4 Displacements

To measure the vertical deflections of the specimens, five vertical displacement transducers were placed along the length of the beam, as shown in Figure 10. Two of the transducers were positioned to measure the displacement at the points of load application, and one transducer was placed at midspan to obtain the maximum deflection. The remaining two transducers were placed 200 mm either side of the connection.

4.3 Test Procedure

Each test commenced with the assembly of the joint. The two halves of the specimen were placed in position in the testing machine, with a central prop holding the joint in position. The bolts were then assembled as shown in Figure 14b, with a load cell placed under the head of each bolt, and a flat washer placed between the load cell and indicating washer positioned as shown. Each bolt was then tightened to the designated pre-tension of 145 kN, corresponding to 60 % proof stress. This tension was achieved by monitoring the gap between the load indicating washer and standard washer. To establish a distribution of bolt tensions which was as uniform as possible, the bolts were tightened in the sequence shown in Figure 15a and 15b for Type A and Type B connections, respectively.

Using the four point bending arrangement, load was applied using a hydraulically actuated ram under displacement control. For each increment, the applied load, the transducers and strain gauges were read and recorded using a Spectra data acquisition system. Once the specimen started to exhibit inelastic behaviour, the increment was applied and the specimen held at this displacement for three minutes to allow the yielding to spread and a true position of static equilibrium to be obtained.

Since the sections were not susceptible to local buckling, the ultimate load of the specimen was limited by either (1) plastic section failure, or (2) connection failure. The ultimate connection failure occurred either when the bolts fractured, or when punching shear failure occurred on the tensile side of the connection. Each specimen was tested until the ultimate failure load was attained. In most cases the end plates formed a yield line mechanism well before the ultimate load was reached. As the tests continued, the end plate deformations increased until the ultimate strength was obtained.

5. Test Results and Discussion

The maximum moment M_u recorded for each test together with the mode of "failure" are shown in Table 5. The following three modes of failure were observed:

- bolt failure when the bolts reach their ultimate tensile load;
- punching shear failure as the end plate shears around the section;
- excessive deformations forcing termination of the test, herein termed "deformation" mode of failure.

The ratios of the experimental maximum moment (M_u) to the nominal full plastic moment (M_n) and the measured plastic moment (M_p), the latter defined as the maximum moment attained in the plastic bending tests, are also given in Table 5.

The graphs detailing the behaviour of the connection specimens during the experiments are presented in Appendix A. In this appendix, three graphs are included for each test as described below, each graph demonstrating a different facet of the connection behaviour.

- Figures A1 to A10 - graphs of the applied bending moment (M) *vs* the measured rotation of the connection (θ_c) and the measured rotation of the section (θ_s) in the region of uniform moment for Type A joints. Figures 17 and 18 show all the moment-rotation curves for the SHS and RHS, respectively.

- Figures A11 to A28 - graphs of the applied bending moment (M) *vs* the measured rotation of the connection (θ_c) and the measured rotation of the section (θ_s) in the region of uniform moment for Type B joints. Figures 19 and 20 show all the moment-rotation curves for the SHS and RHS, respectively.

- Figures A29 to A36 - graphs of the measured connection rotation (θ_c) *vs* the measured separation of the plates (p_s) at the toe of the weld near the bottom flange.

The values of the connection rotation in Figures A1 to A36 have been determined using the difference between the rotation of the section (θ_s) calculated using the beam strains, and the total rotation (θ_t) of the connection measured using the lateral transducers as described previously ($\theta_c = \theta_t - \theta_s$), see Figure 3.

5.1 Type A (Eight-Bolt) Connections

The ultimate failure modes for Type A connections, shown in Table 5, demonstrate that for the square hollow sections the dominant mode of failure was tensile bolt failure. By comparison, the dominant failure mode for the rectangular sections was punching shear along the bottom flange at the toe of the weld, as can be seen in Figure 16. The high relative strengths and low rotations for the latter connections suggest that this type of connection is comparatively stiff.

The Type A connections were initially stiff with the moment-rotation relationship closely resembling that of the beam pure section. As the loads increased, the rotation in the joint increased at an increasing rate, indicating a decrease in connection stiffness. The magnitude of this joint rotation is dependent on the end plate variables of plate thickness and bolt position. A comparison between the plate separation (p_s) and the joint rotation (θ_c) reveals a linear relationship between the two (see Figure 21 later). The point at which the stiffness begins to decrease markedly corresponds to the point at which the plate separation increases at a measurable rate, and to the point at which there is a marked increase in the loads in the tensile (bottom) bolts.

The effects of the end plate thickness (t_p) and the distance from the bolts to the perimeter of the section (s_o) on the moment rotation behaviour are shown in Figures 17 and 18 for the square and rectangular sections, respectively. An increase in the plate thickness (t_p) increases the rigidity which subsequently increases the strength and stiffness of the connection (compare SHS specimens #3 (12mm), #1 (16mm) and #4 (20mm), and RHS specimens #5 (12mm), #2 (16mm) and #6 (20mm)). The effect of altering the bolt location has a similar effect, with the rigidity of the end plate increasing, as the bolts are positioned nearer to the section (compare SHS specimens #1, #7 and #8 and RHS specimens #2, #9 and #10). With respect to specimens #1, #4, #6, #7 and #10, although the ultimate failure modes were classified as either bolt failure or punching shear, extensive yielding occurred in the section itself. This is reflected in the high ratios M_u/M_p given in Table 5 for theses specimens.

5.2 Type B (Four-Bolt) Connections

In most cases the ultimate failure mode for Type B connections was tensile bolt failure, but for the thinner more flexible plates the tests were stopped due to excessive deformations in the end plates. The ultimate failure loads rarely exceeded $0.6M_p$ suggesting that for the range of section sizes and end plate thicknesses considered in this study, it is not possible to realise the full section capacity of the connected beam using this type of connection.

As in the Type A connections, the Type B connections have an initial stiffness closely resembling that of the pure beam section, but the point at which the rate of rotation increases occurs at a considerably lower load than for the corresponding Type A connection. The rate of joint rotation or stiffness of the connection also increased as the load increased, but at a greater rate than for the corresponding Type B connection.

The rate of the joint rotation was again dependent on the end plate variables of thickness and bolt position, with the point at which the stiffness clearly begins to decrease corresponding to the point at which a measurable plate separation occurs.

The effect of changes in the end plate width (W_p) and thickness (t_p) is shown in Figures 19 and 20 for the square and rectangular sections, respectively. An increase in plate thickness (t_p) increases the stiffness and the strength of the joint (compare SHS specimens #11, #12, and #13, and RHS specimens #14, #15 and #16). This increase can be attributed to the increased stiffness of the end plate. An increase in the plate width (W_p) (corresponding to moving the position of the bolts away from the line of the webs as denoted by the parameter *c* in Table 2) reduces the stiffness and strength of the joint (compare SHS specimens #12 and #18, and RHS specimens #15 and #21). The effect of the position of the bolts is further demonstrated through their proximity to the section flange (parameter s_o in Table 2). As the bolts were moved closer to the flange of the section, the connection stiffness and strength also increased (compare SHS specimens #23, #12 and #24, and RHS specimens #25, #15 and #26).

For the test specimens with the 12 mm end plate (specimens #11, #14, #17 and #20), a mechanism formed in the plate when the bolt loads were well below the ultimate capacity. This mechanism was such that the load transfer to the bolts was induced by membrane forces in the deformed and plate, and ultimate fracture of the bolts would eventually occur at very high rotations. These tests were stopped due to the large deformations experienced in the connection.

Test #13 and #19, corresponding to square hollow sections with a 20 mm end plate, were initially carried out using ungalvanized Metric Grade 8.8 bolts produced by Bremick Pty Ltd. These tests have been reported as #13* and #19* in Table 5, the ultimate load of these tests was limited by bolt failure through the shearing of the bolt thread. It was therefore decided to repeat these tests using corresponding structural grade galvanized bolts from Ajax Fasteners (1991). The results of these additional two tests are reported

as #13 and #19 in Table 5. The connection failure modes pertaining to these later tests were 10 percent higher than the earlier nominally identical tests (#13* and #19*) with the bolts failing through tensile fracture as expected.

5.3 Discussion

The moment-rotation curves for both the Type A and Type B connections clearly demonstrate the non-linearity that occurs in these configurations of moment end plate connections. As discussed in more detail hereafter, the moment-rotation behaviour is also affected by the initial tension in the bolts, and the distortion in the plates due to the welding process.

Pre-tensioning of the bolts in the connection places a compressive force into the end plates. Until this compressive pre-load is exceeded by the superimposed tensile loads in the bolts on the tensile side of the neutral axis, (resulting from the moment loading), the forces in the bolts themselves will change little. When this pre-load is exceeded, however, the tensile bolts will begin to take up the additional load. This phenomenon was demonstrated in the measured bolt loads, where a significant increase in the rate of loading of the tensile bolt was observed. At the same time the connection rotation and the plate separation also started to increase rapidly. The pre-tensioning of the bolts increases the initial stiffness of the connection but will have negligible effect on the ultimate strength of the connection.

During the welding process, the end plates distort, causing the edges of the plate to curve towards the weld. The magnitude of the distortion of the edge of the plate relative to the centre depends on the end plate thickness. The distortions ranged from 1 mm for the thickest (20 mm) plate to 3 mm for the thinnest (12 mm) plate. When the connection is assembled, the prestressing of the bolts introduces stresses into the end plates, which reduce the load required to initiate yield. Again, the effect on the ultimate load of the connection will be minimal, but a reduction in the stiffness of the connection may occur due to this early yielding in the end plate.

The relationship between the measured plate separation (p_s) and the connection rotation (θ_c) is shown in Figure 21 for Type B connections. This relationship is linear and has been proven by analysis of the correlation coefficients (Freund., 1988). The correlation coefficient and corresponding linear relationship for each test, along with the background theory are given in Appendix C.

The moment-rotation curves for the comparative beam tests (without a central connection) are shown in Figure 22. The nominal full plastic

moments of 87 kN.m and 102 kN.m for the SHS and RHS, respectively, are also indicated on the figure as are the corresponding ultimate moments. The tests were stopped once a clear yield plateau had formed, and excessive deformations experienced. The ultimate moments for the sections were 30 % higher than the nominal full plastic moments. Figure 23 demonstrates that the effect of welding on the section behaviour is minimal and can be dismissed as having an effect on the strength of the section.

5.4 Bjorhovde Classifications

The connections tested experimentally have been classified in terms of their moment-rotation behaviour for both the strength and serviceability (stiffness) limit states, using the non-dimensional classification scheme of Bjorhovde *et al*. (1990), (see Section 2 and Figure 2 previously). The results of all connections tested are plotted in Figures 24 and 25 for Type A connections, and in Figures 26 and 27 for Type B connections, along with the corresponding Bjorhovde limits. The values of M_p used to non-dimensionalise the results were determined experimentally from the comparative beam tests (Figure 22). The ultimate plastic moments M_p are therefore 119 kN.m and 138 kN.m for the square and rectangular sections, respectively.

For the strength limit state, all the Type A connections, with the exception of specimen #5, were classified as rigid connections (Figures 24 and 25). Specimen #5 was classified as a semi-rigid connection because the non-dimensionalised moment did not exceed 0.7. In terms of serviceability, specimens #1, #2, #4, #6, #7, #9 and #10 were classified rigid, as their moment-rotation curves consistently fell within the rigid zone. The remaining specimens (#3, #5, and #8) were classified as semi-rigid because a significant portion of their moment-rotation behaviour fell within the semi-rigid zone.

Although the strength and stiffness of the Type B connections (four bolts) varied greatly, all the connections were classified as semi-rigid for both the serviceability and strength limit states (Figures 26 and 27).

Comparisons of the non-dimensionalised results for similar SHS and RHS connections (same plate thickness and bolt position) are shown in Figure 28. There is a clear correlation between the connections with the same plate parameters, as can be seen by comparing the square hollow sections #11 to #13 with the rectangular hollow sections #14 to #16. This comparison demonstrates the dependency of the non-dimensional moment-rotation behaviour on the plate parameters rather than on the section properties.

6. Conclusions

This report has described a test programme on the behaviour of bolted end plate connections, with either eight or four bolts, joining square and rectangular hollow section tubular members. The moment-rotation behaviour of the connections has been presented to enable the response to be modelled correctly in advanced analysis of frames. The yield loads and ultimate strengths of the connections will be used for the calibration of theoretical and design models for these connection types.

The tests showed that the rigidity of the end plate has a dominant effect on the moment-rotation behaviour of the connection. The degree of rigidity depends primarily upon the thickness of the end plate and the number of bolts. An increase in the thickness of the plate causes an increase in the stiffness and strength of the connection, while the connections containing eight bolts achieved higher stiffness and strength than the corresponding four bolt connections. The location of the bolts with respect to the perimeter (flange or web) of the section also affects the rigidity of the end plate. The closer the bolts are located to the perimeter, the more rigid the plate, and the greater the strength and stiffness of the connections. In the Type B (four bolt) connections, a decrease in the stiffness and strength of the joint occurred as the bolts were moved perpendicularly away from the webs (resulting in the need for a wider end plate).

The connection ultimate failure modes observed in the tests comprised of either tensile bolt failure or punching shear (tearing out) of the tensile section flange from the end plate. While the ultimate failures occurred in the connections themselves for the stiffer Type A (eight bolt) series, extensive yielding of the connected beam section was also apparent at the ultimate load. Local buckling failure of the sections did not occur because of their compact nature.

Using the classification scheme proposed by Bjorhovde *et al*. (1990), the experimentally determined moment-rotation curves indicate that for the strength limit state the Type A connections are predominantly rigid, and the Type B connections are predominantly semi-rigid. For the serviceability (stiffness) limit state, the Type A connections are classified as rigid for the thicker end plates but semi-rigid for the thinner end plates. Considering the nature of the entire moment-rotation responses, the Type B connections can all be classified as semi-rigid.

7. References

AISC (1992). *Design Capacity Tables for Structural Steel Hollow Sections*, Australian Institute of Steel Construction, Sydney, Australia.

Ajax Fasteners (1992). *Fasteners Handbook - Bolt Products*, Richmond, Victoria, Australia.

Bjorhovde, R., Brozzetti, J. and Colson A., (1990). A Classification System for beam to column connections. *Journal of Structural Engineering*, ASCE, **116**(11), 3059-76.

CEN (1992). *ENV 1993–1–1 Eurocode 3, Design of Steel Structures, Part 1.1 — General Rules and Rules for Buildings*, European Committee for Standardisation, Brussels, 1992.

Freund., J. E. (1988). *Modern Elementary Statistics*. 7th edition, Prentice Hall, Sydney.

Grundy, P., Thomas ,I. R. and Bennetts, I. D., (1980). Beam-to-Column Moment Connections. *Journal of Structural Engineering*, ASCE, **106**(1), 313-330.

Kato, B. And Hirose, R. (1985). Bolted Tension Flanges Joining Square Hollow Section Members. *Journal of Structural Engineering, ASCE*, **111**(5), 163-177.

Kato, B. And Mukai, A. (1991). High Strength Bolted Flanges Joints of SHS Stainless Steel Columns. *International Conference on Steel and Aluminium Structures, Singapore, May 1991*.

Kukreti, A. R., Ghassemieh, M. and Murray T. M., (1990). Behaviour and Design of Large-Capacity Moment End Plates. *Journal of Structural Engineering, ASCE*, **116**(3), 809-828.

Packer, J. A., Bruno, L., Birkemoe, P. C. (1989). Limit Analysis of Bolted RHS Flange Plate Joints. *Journal of Structural Engineering, ASCE*, **115**(9), 2226-2241.

SA (1981a). *AS 1252-1981: High-strength Steel Structural Bolts with Associated Nuts and Washers for Structural Engineering*. Standards Australia, Sydney.

SA (1981b). *AS 3678-1981: Structural Steel - Hot-rolled plates, floorplates and slabs*. Standards Australia, Sydney.

SA (1990). *AS 4100-1990: Steel Structures*. Standards Australia, Sydney.

SA (1991a). *AS 1163-1981: Structural Steel Hollow Sections*. Standards Australia, Sydney.

SA (1991b). *AS 1391-1991: Methods for Tensile Testing of Metals*. Standards Australia, Sydney.

SA (1991c). *AS 1554.1-1991: Structural Steel Welding - Part 1: Welding of Steel Structures*. Standards Australia, Sydney.

8. Notation

θ	rotation
$\bar{\theta}$	non-dimensionalised rotation
θ_c	connection rotation
θ_s	section rotation
θ_t	total joint rotation
a_e	distance from edge of end plate to centre of bolt hole
b	width of section
c	distance from line of section webs to centre of bolt hole
d	depth of SHS or RHS
D_p	depth of end plate
E	Young's modulus of elasticity
e_u	percentage elongation at ultimate strength
f_u	measured tensile strength
f_{un}	nominal tensile strength
f_y	measured yield stress
f_{yn}	nominal yield stress
g	distance of bolt hole from adjacent face of section
I_b	second moment of area of beam section
l	length of lever arm from support to load point in tests
l_B	length of bolts (length of shank plus thread)
l_r	horizontal distance from connection to lateral transducer measuring rotation
l_t	vertical distance between lateral transducers measuring rotation
L_b	length of beam for Eurocode 3 classification
$\bar{m}$	non-dimensionalised moment
M	bending moment
M_p	measured full plastic bending moment of section
M_u	measure ultimate connection moment
M_n	nominal full plastic bending moment of section
P	load applied in test
p_s	plate separation
P_u	measured ultimate tensile load of a bolt
s_o	distance from section flange to centre of bolt hole
t	thickness of section
t_p	thickness of end plate
W_p	width of end plate

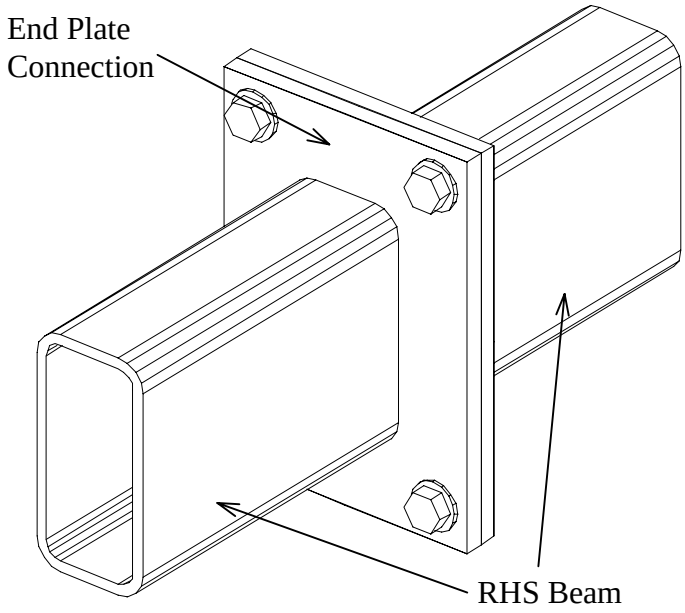

(a) Beam Splice Connection

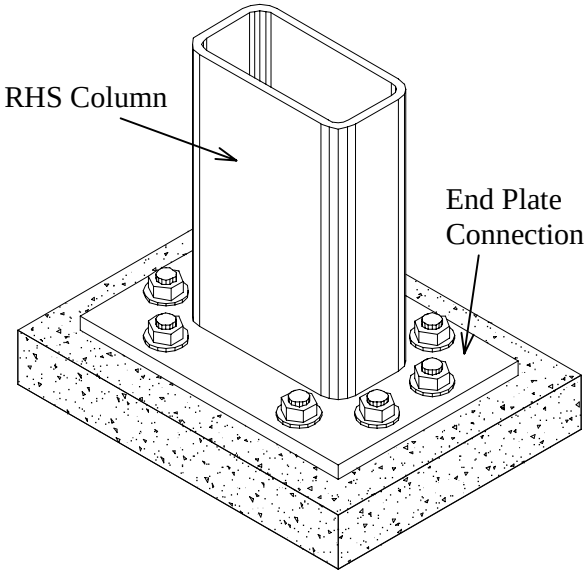

(b) Column Base Plate Connection

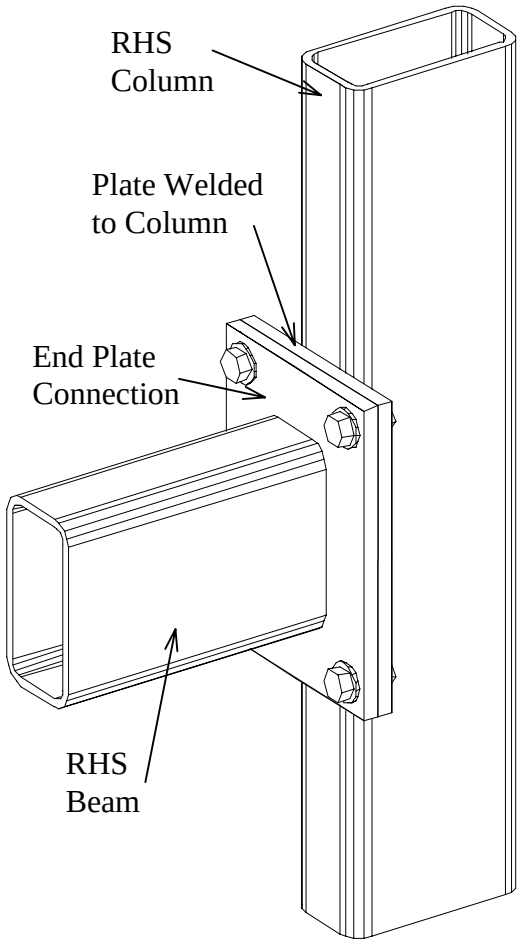

(c) Beam - Column Connection

Figure 1 - Typical End Plate Connections

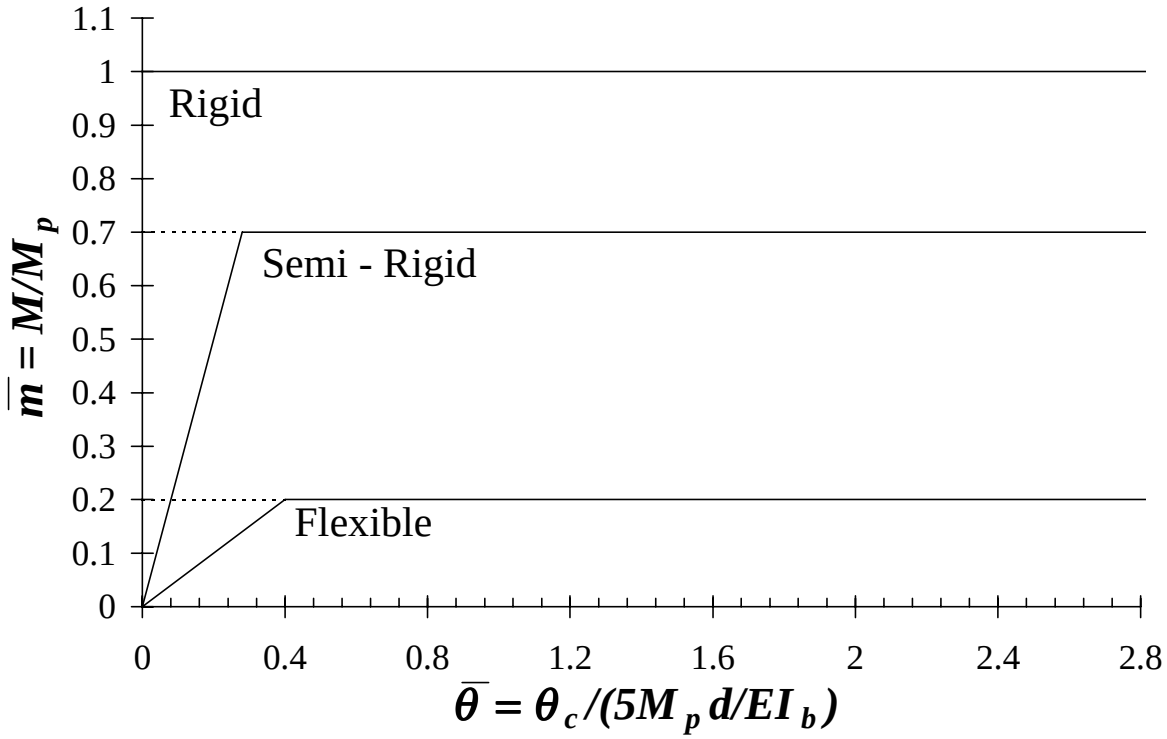

Figure 2 - Bjorhovde Classification Scheme

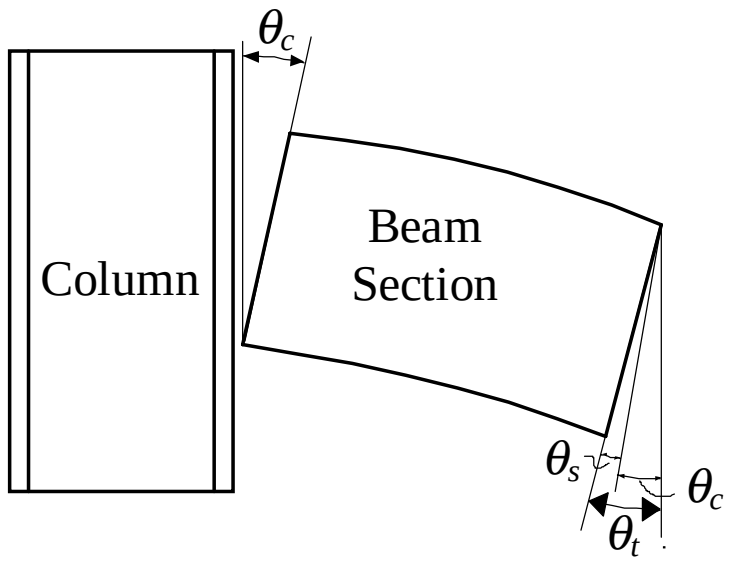

$$\theta_t = \theta_s + \theta_c$$

Figure 3 - Rotation Definitions

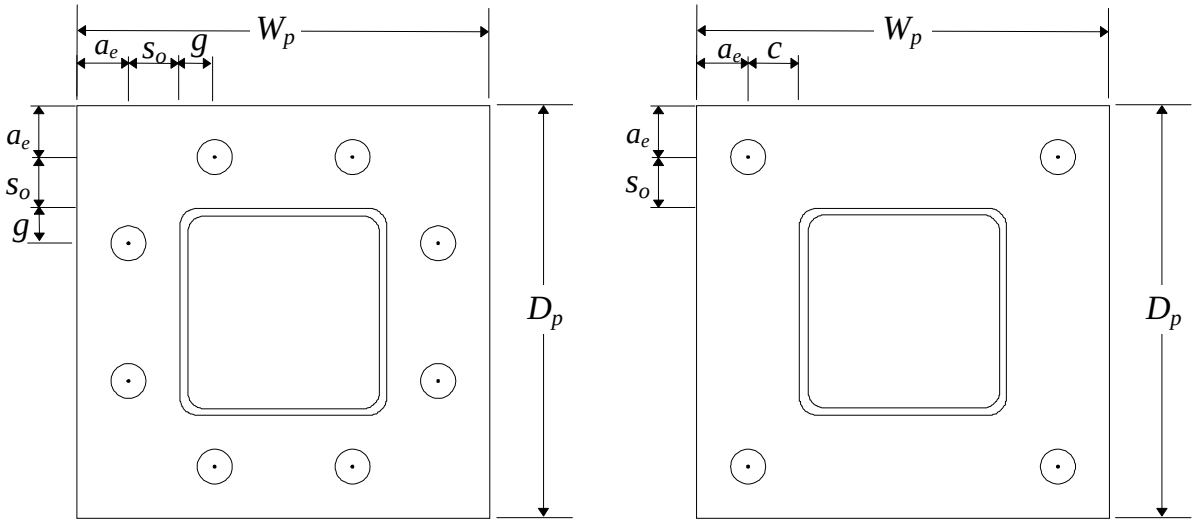

(a) Type A **(b) Type B**

Figure 4 - Flange Plate Dimensions

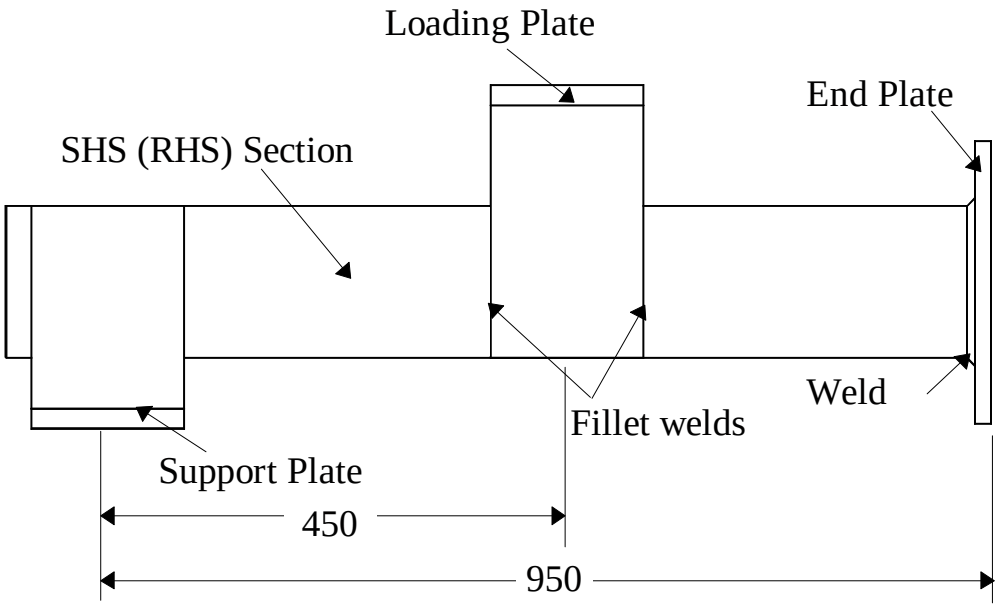

Figure 5 - Specimen Layout

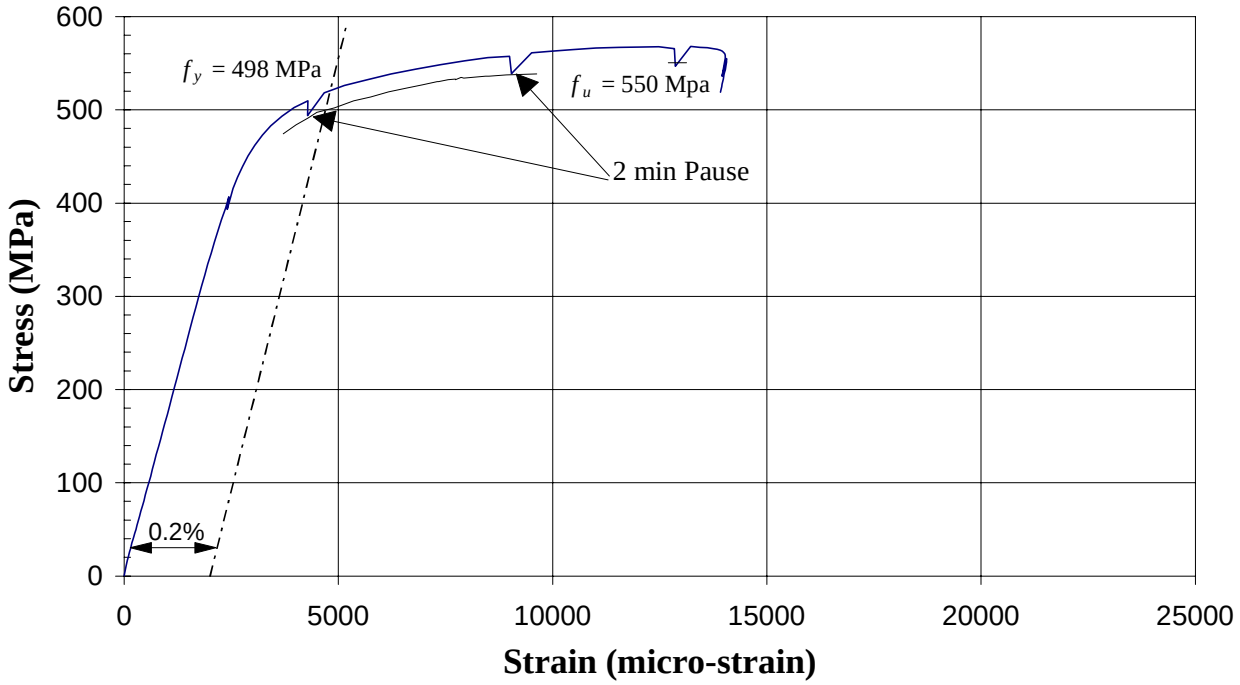

Figure 6 - Typical Stress-strain Curve for Section Corner

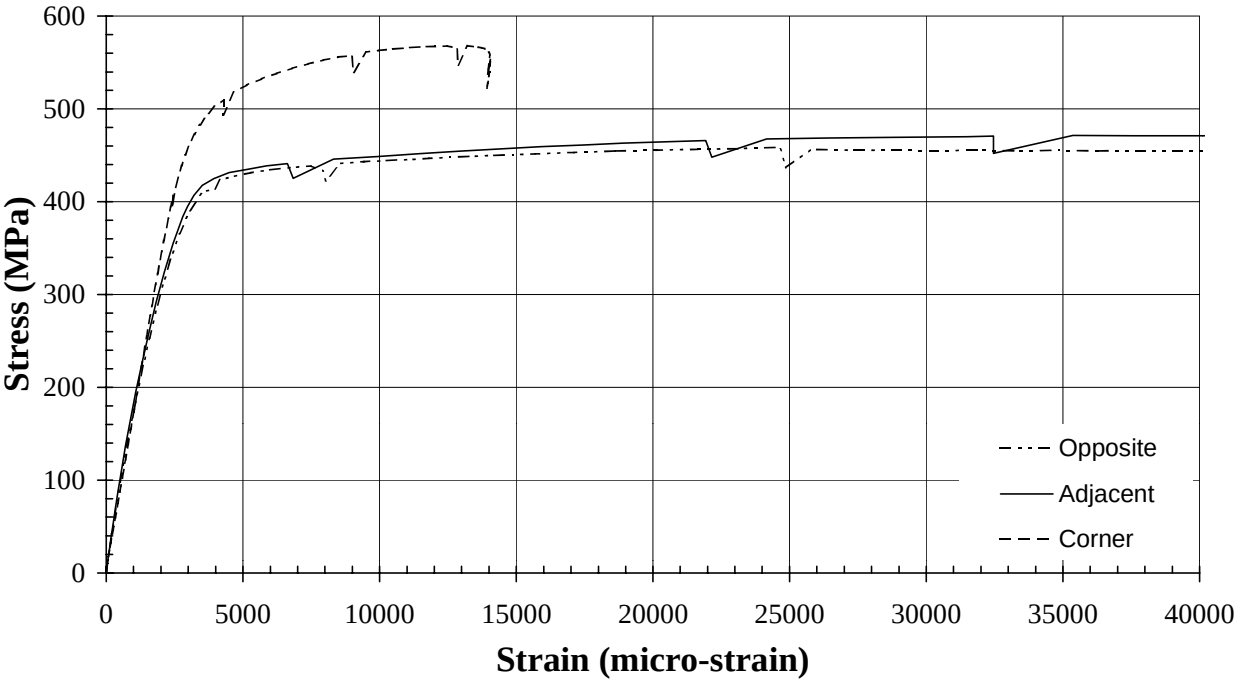

Figure 7 - Typical Stress-strain Curves for Section

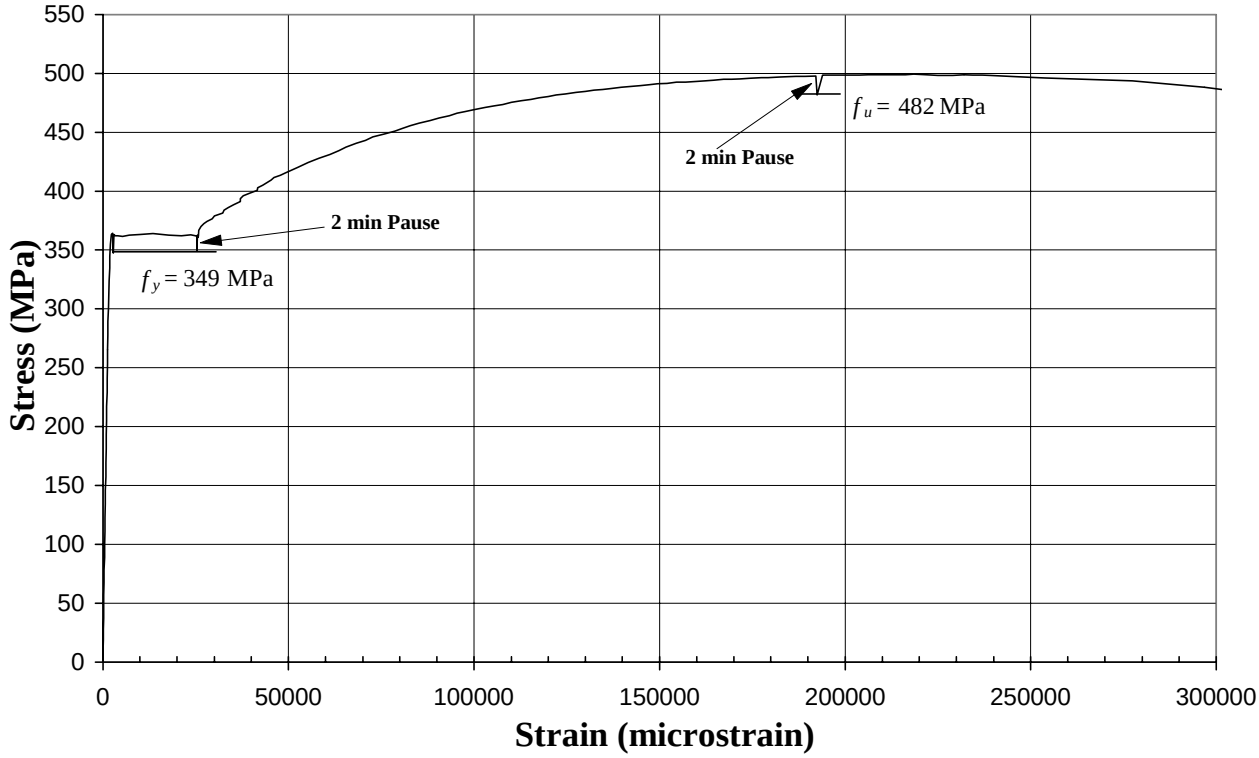

Figure 8 - Stress-strain Curve for Plate

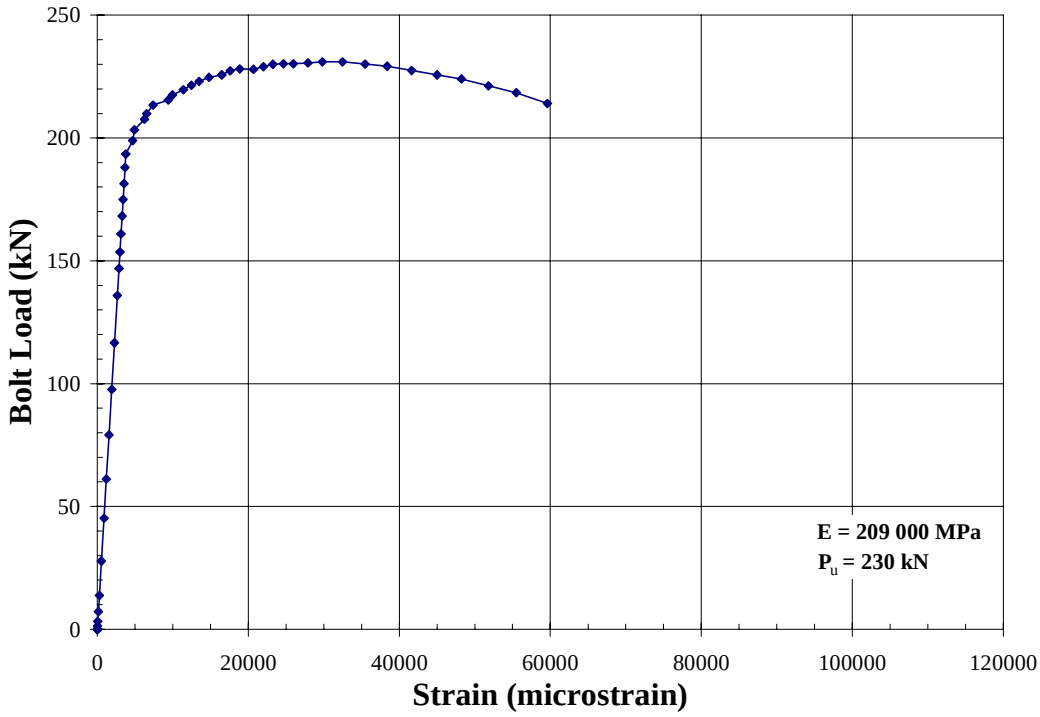

Figure 9 - Load-strain Curve for Bolts

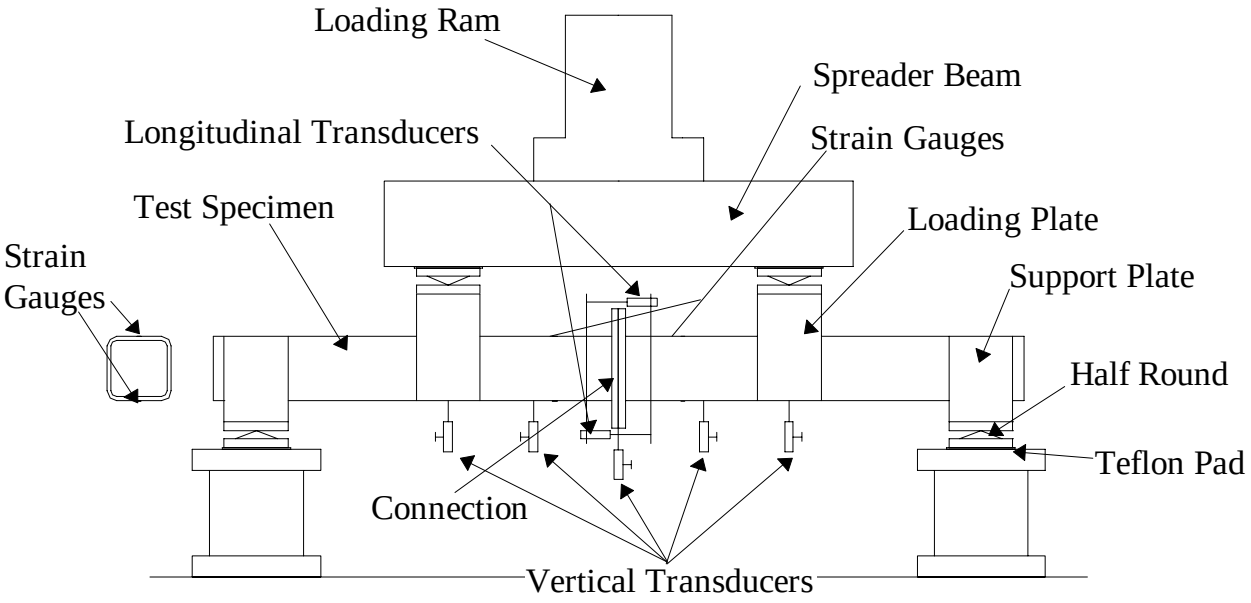

Figure 10 - Schematic View of Testing Rig

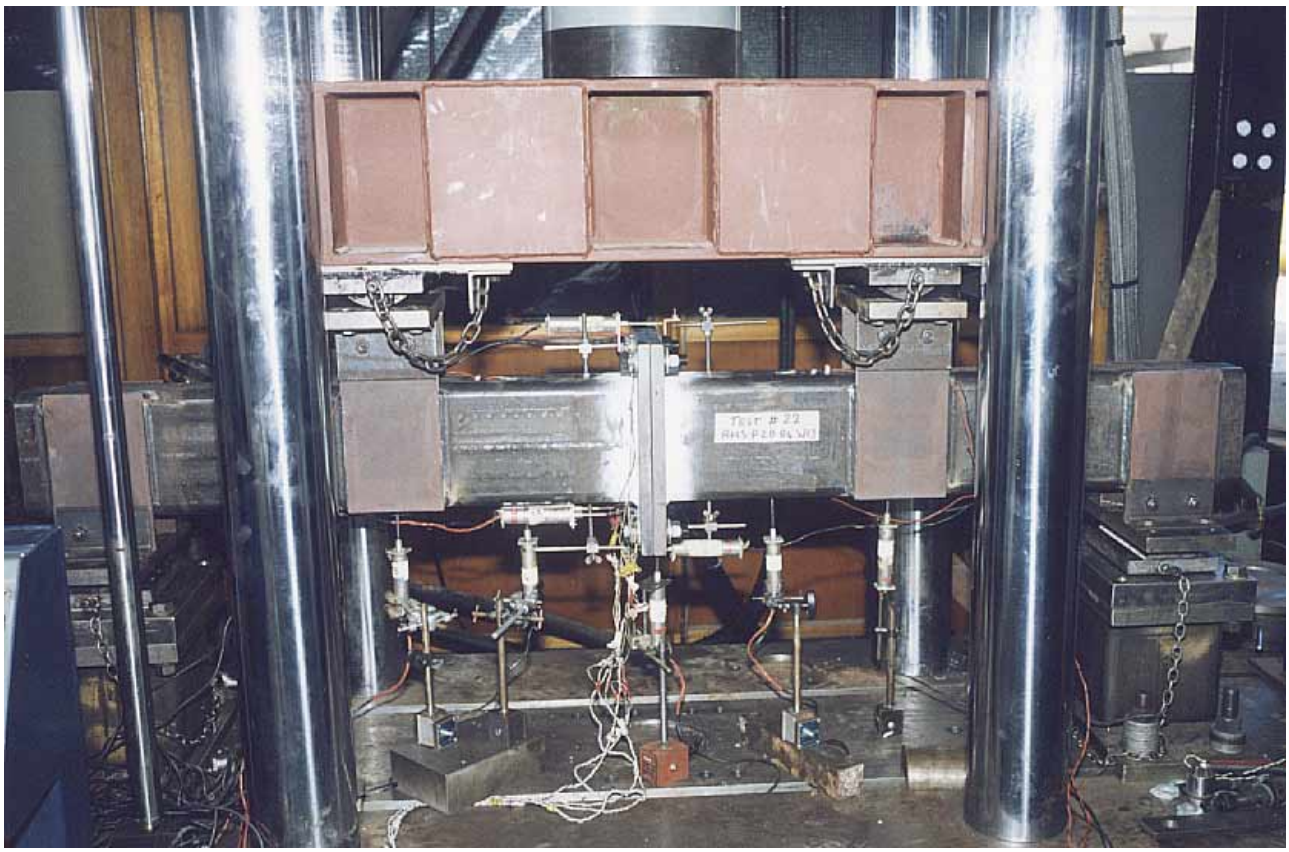

Figure 11 - Test Specimen in Testing Rig

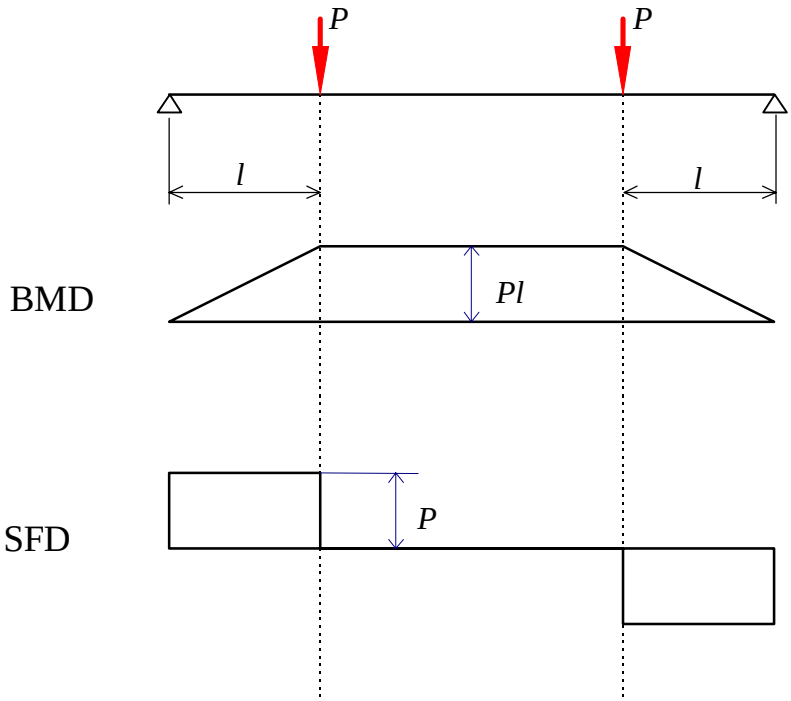

Figure 12 - Bending Moment and Shear Force Diagrams

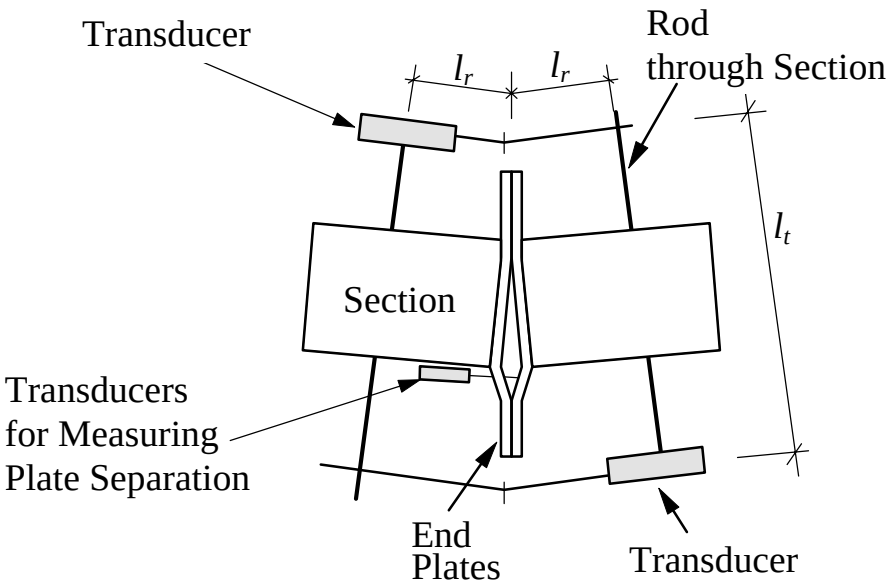

Figure 13 - Total Rotation Measurement

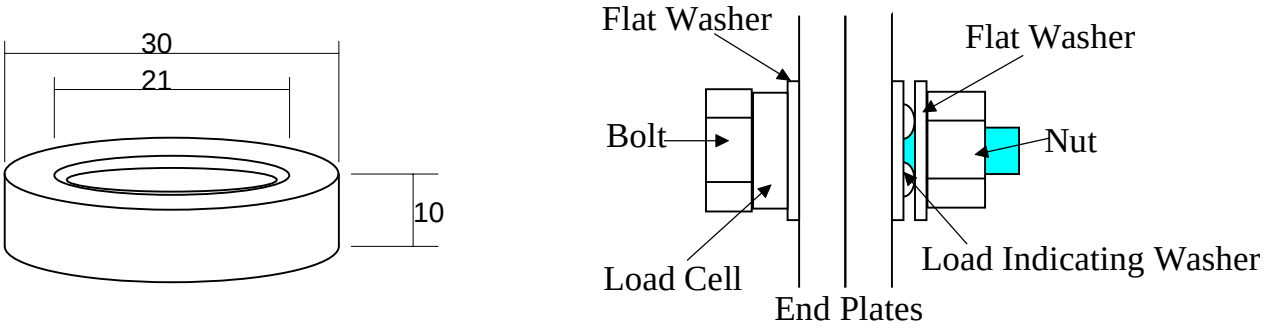

(a) Load Cell

(b) Bolt Assembly

Figure 14 - Load Cell and Bolt Assembly Details

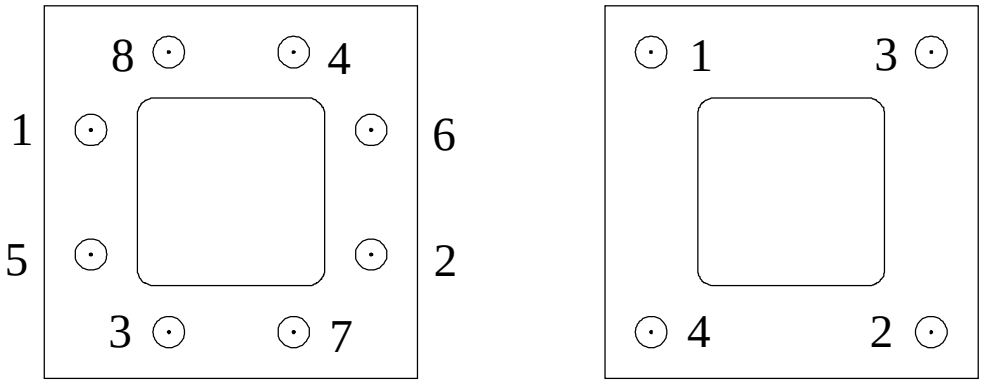

(a) Type A

(b) Type B

Figure 15 - Bolt Tightening Sequence

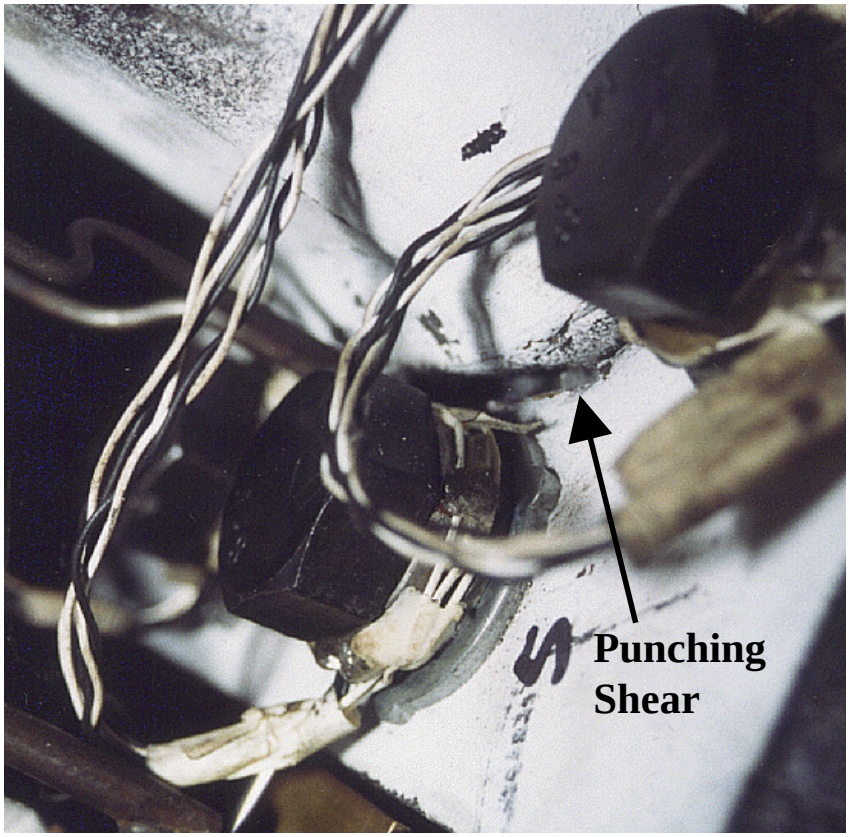

Figure 16 - Plate Punching Shear

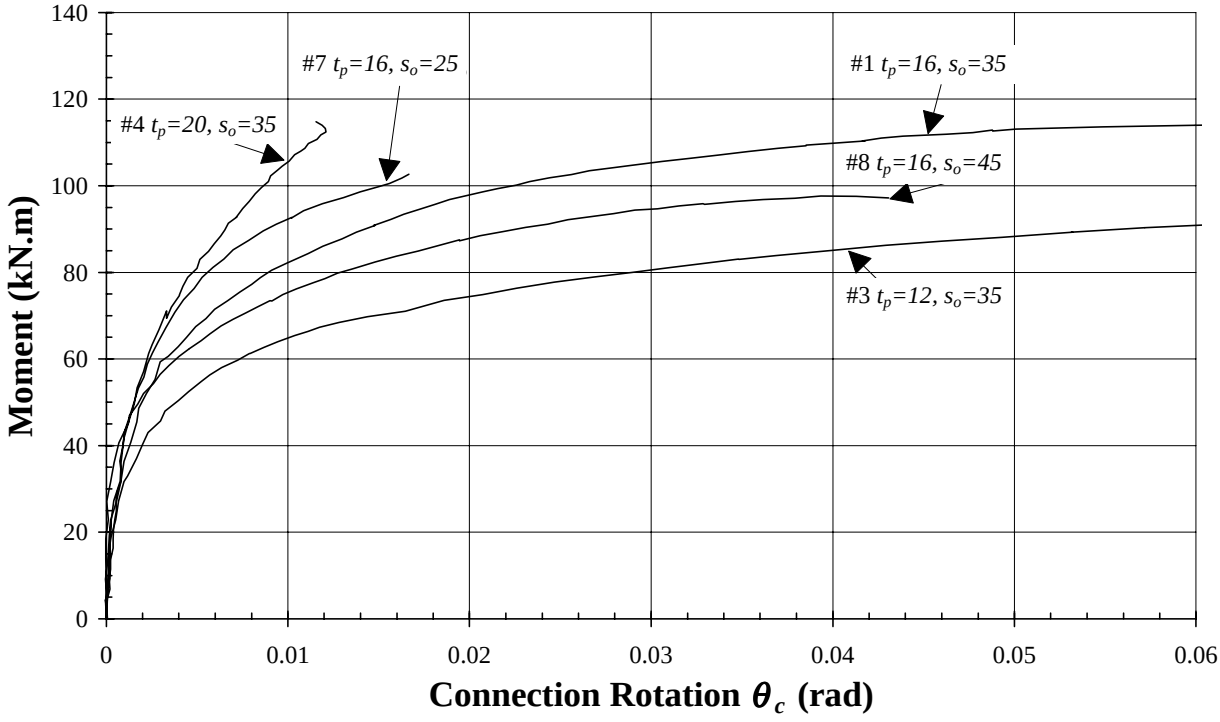

Figure 17 - Moment Rotation Curves -Type A, SHS

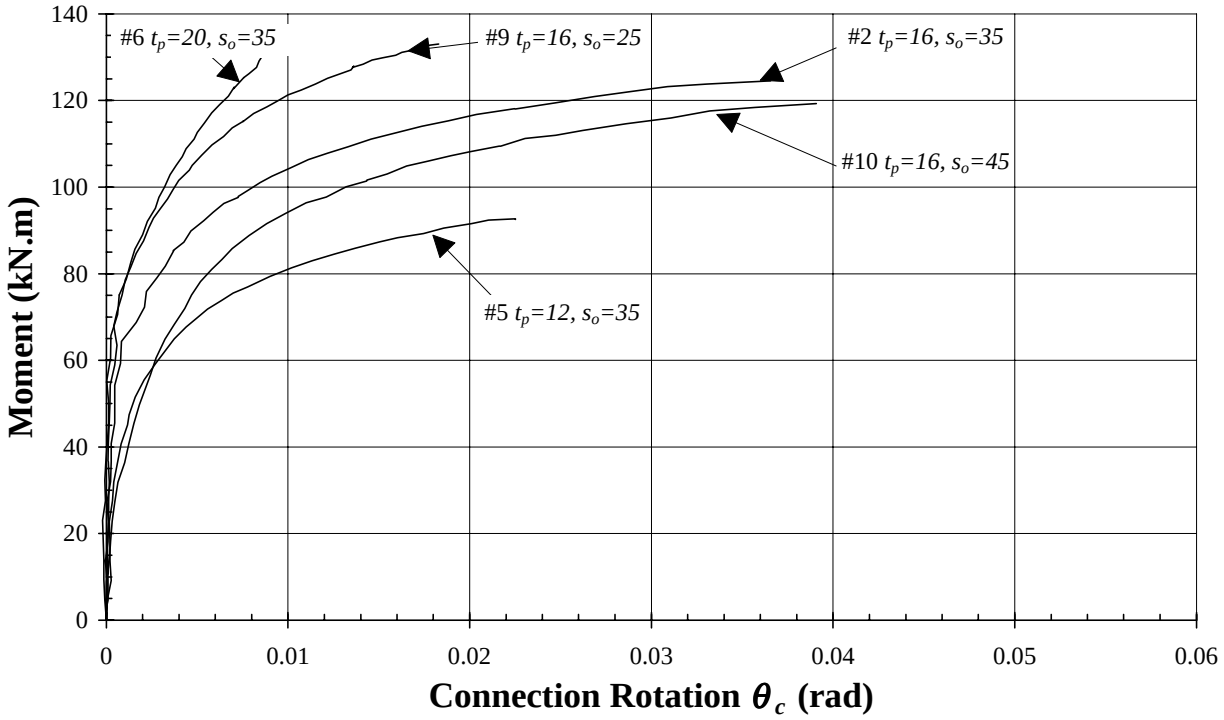

Figure 18 - Moment Rotation Curves -Type A, RHS

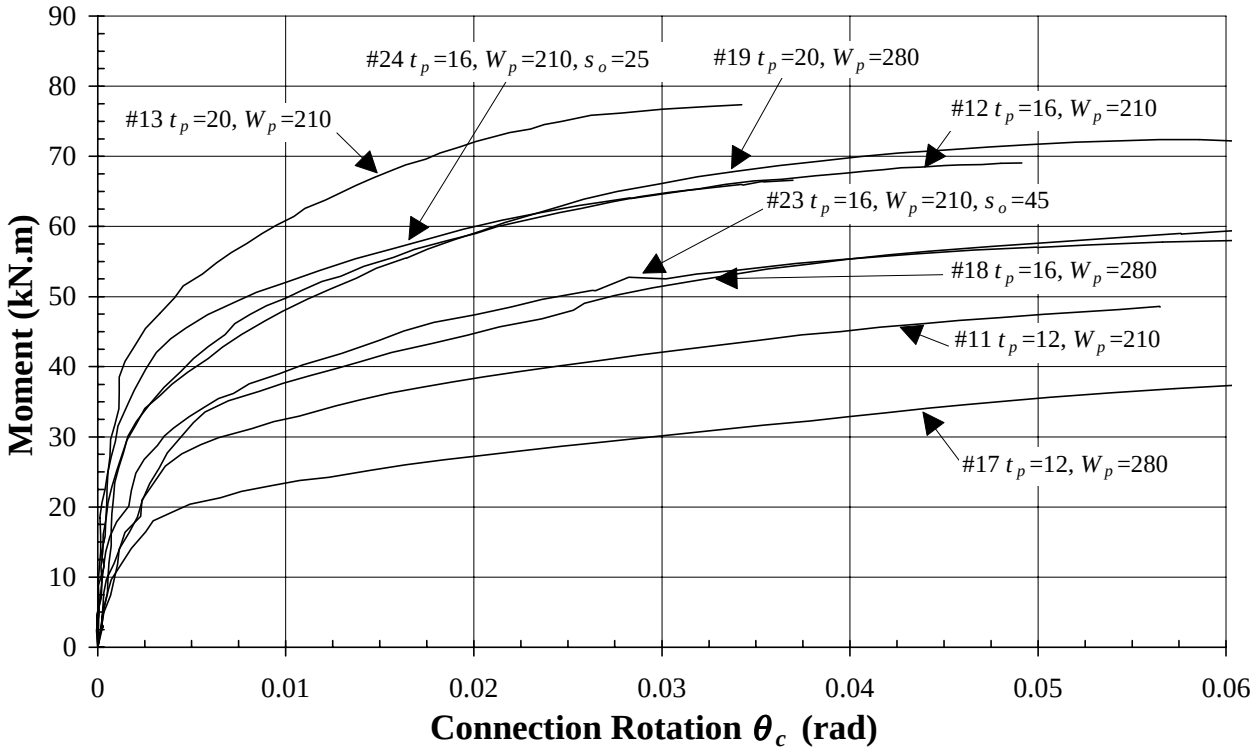

Figure 19 - Moment Rotation Curves -Type B, SHS

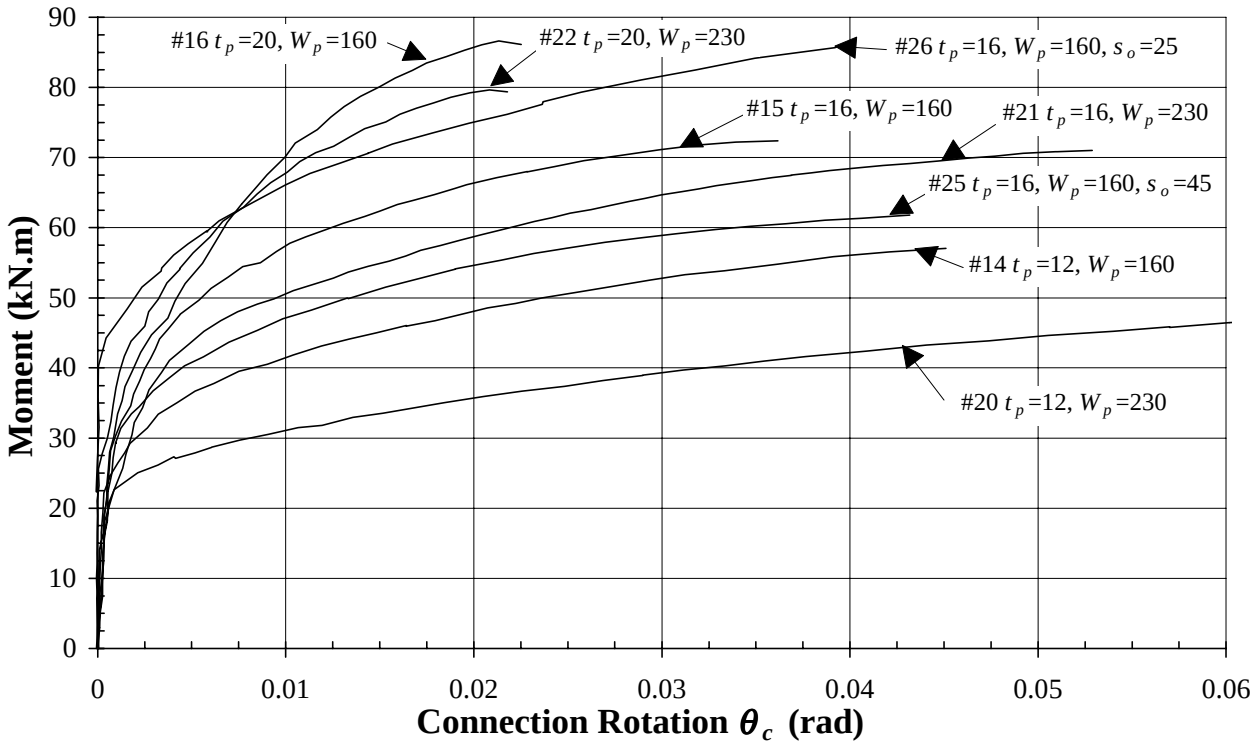

Figure 20 - Moment Rotation Curves -Type B, RHS

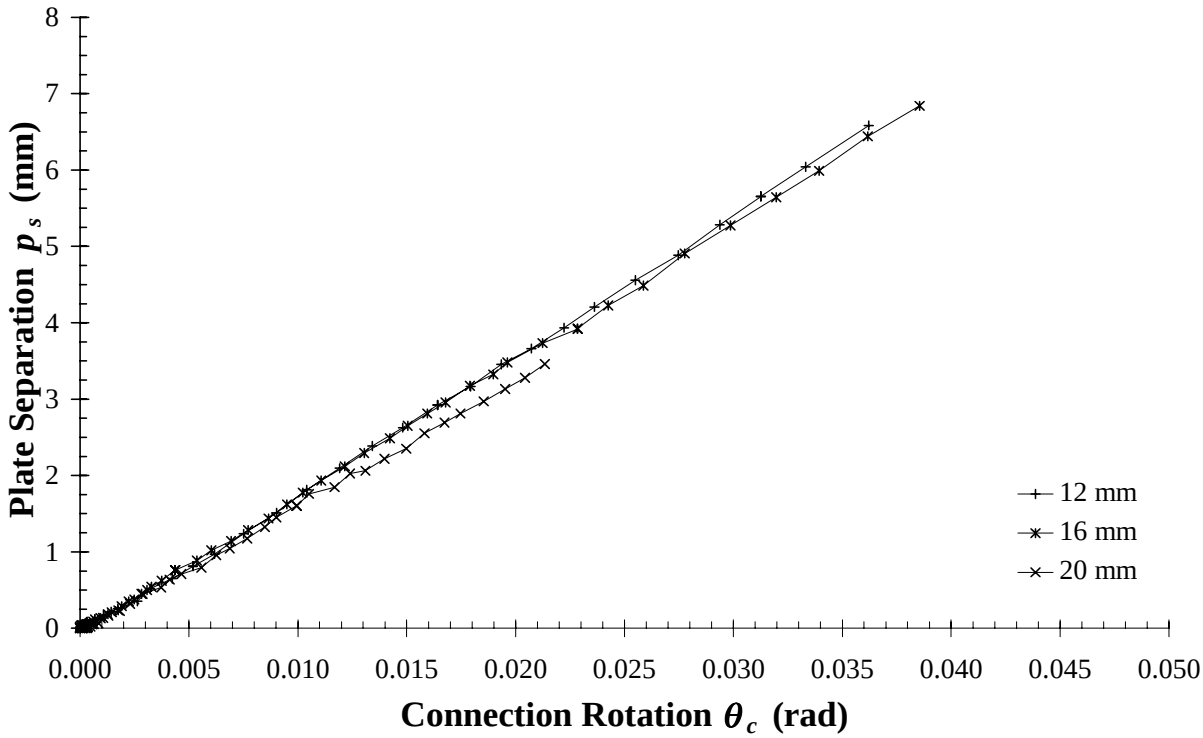

Figure 21 - Plate separation vs connection rotation
(Type B, RHS, W_p=160 mm)

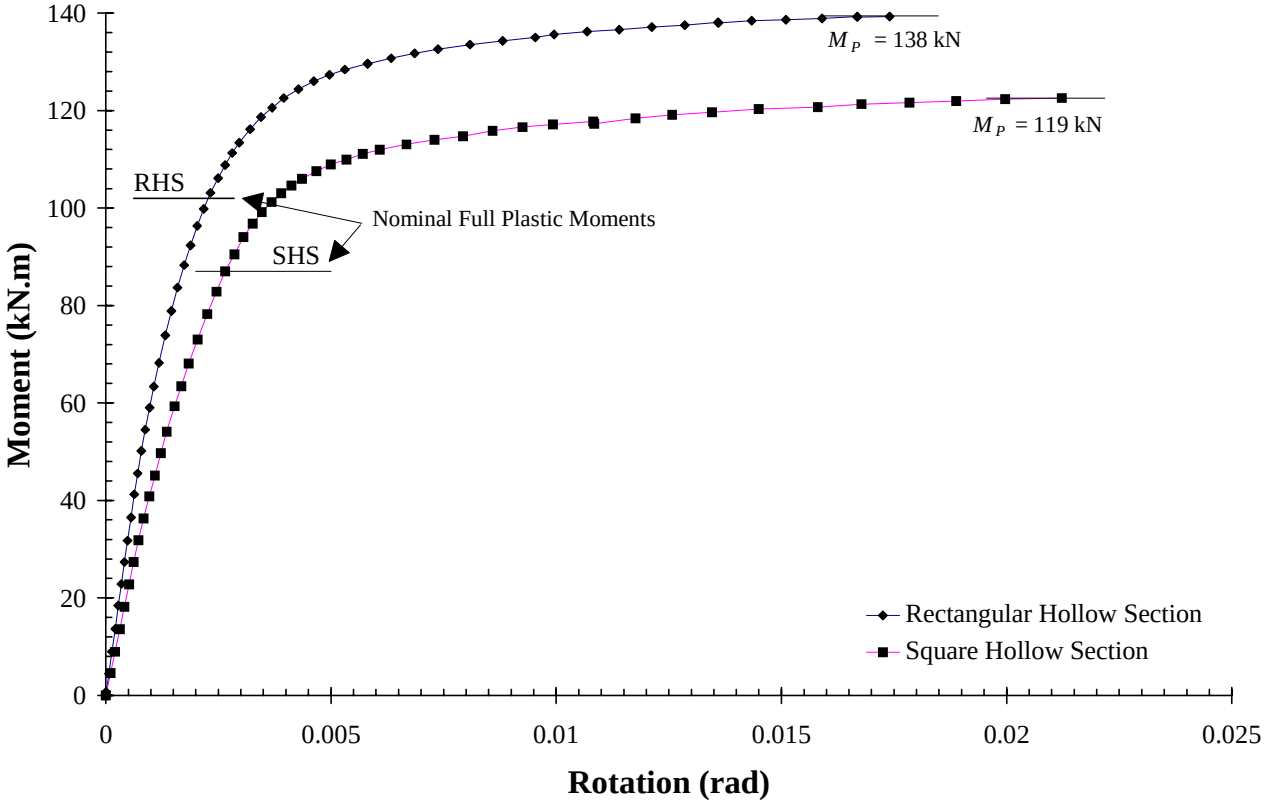

Figure 22 - Section Bending Tests

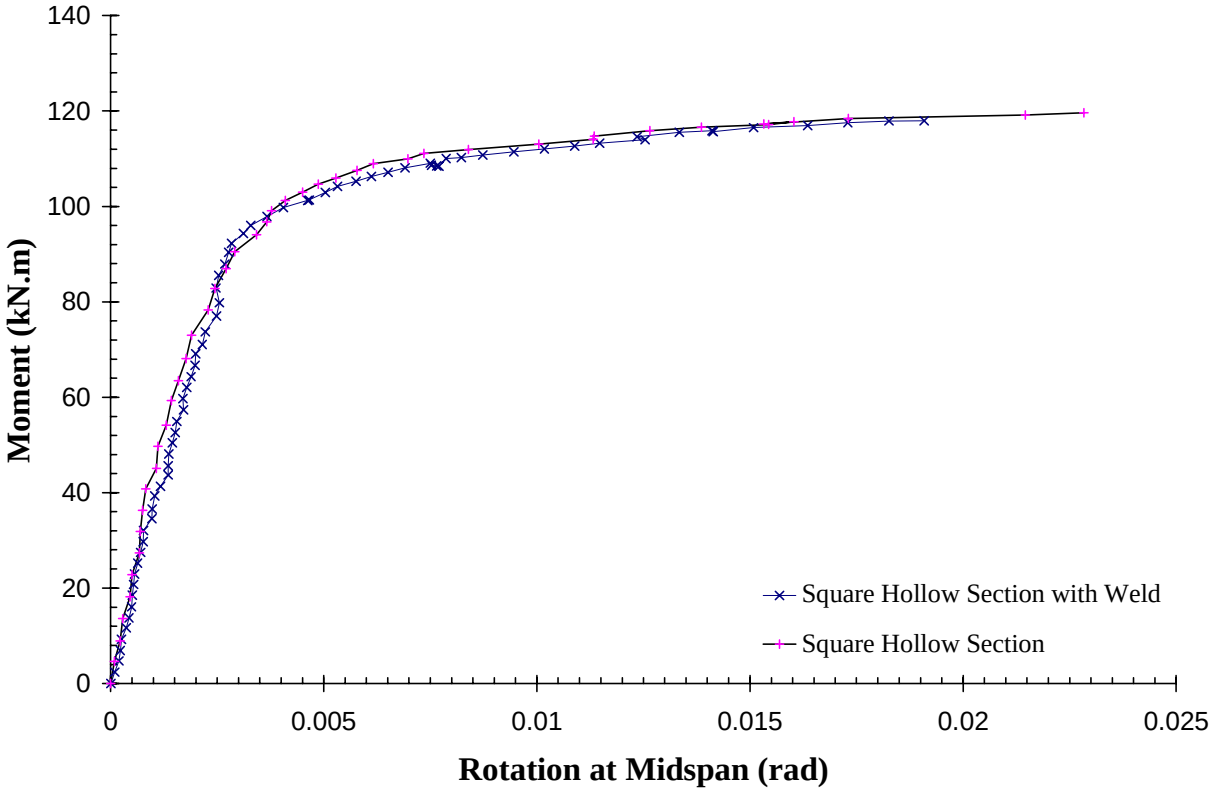

Figure 23 - Comparative Weld Test, SHS

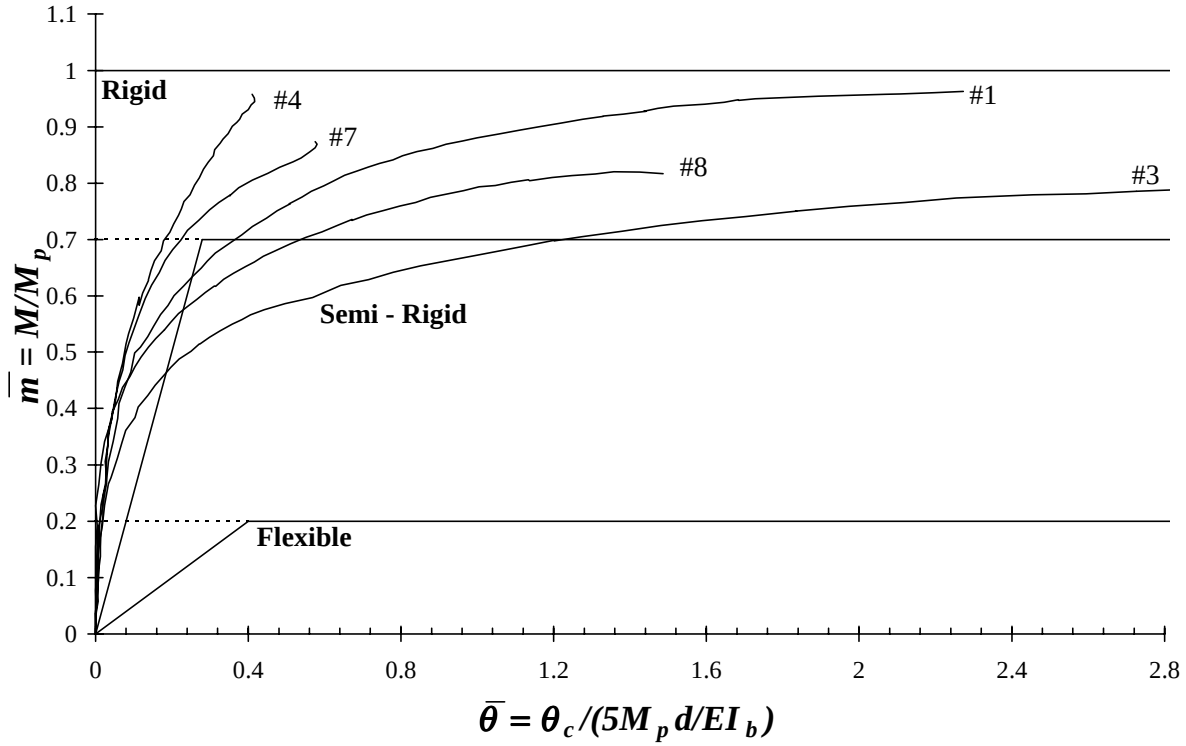

Figure 24 - Bjorhovde Classification -Type A, SHS

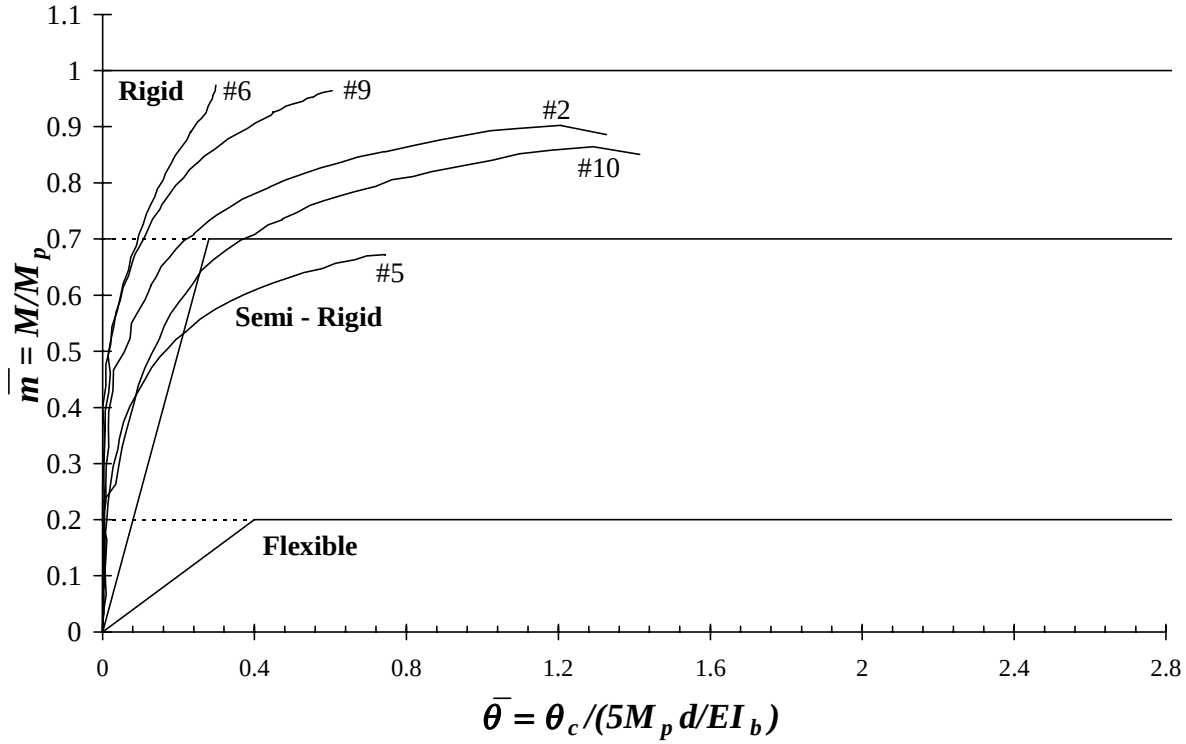

Figure 25 - Bjorhovde Classification -Type A, RHS

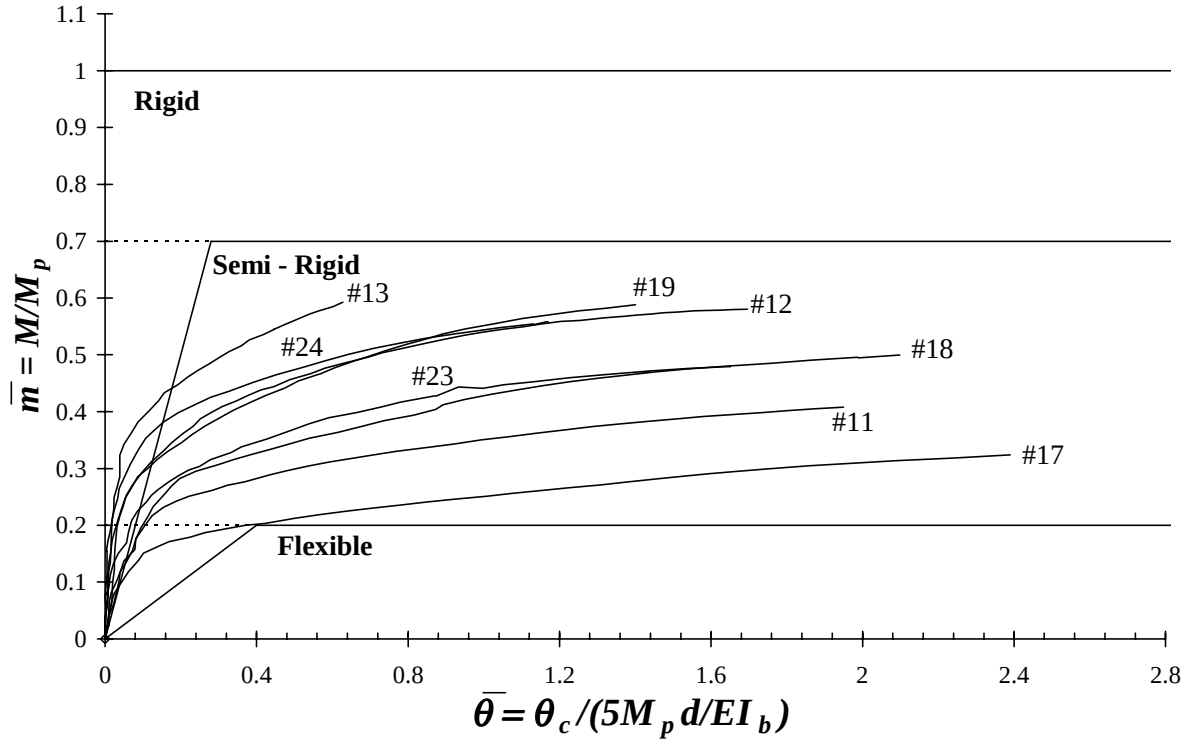

Figure 26 - Bjorhovde Classification -Type B, SHS

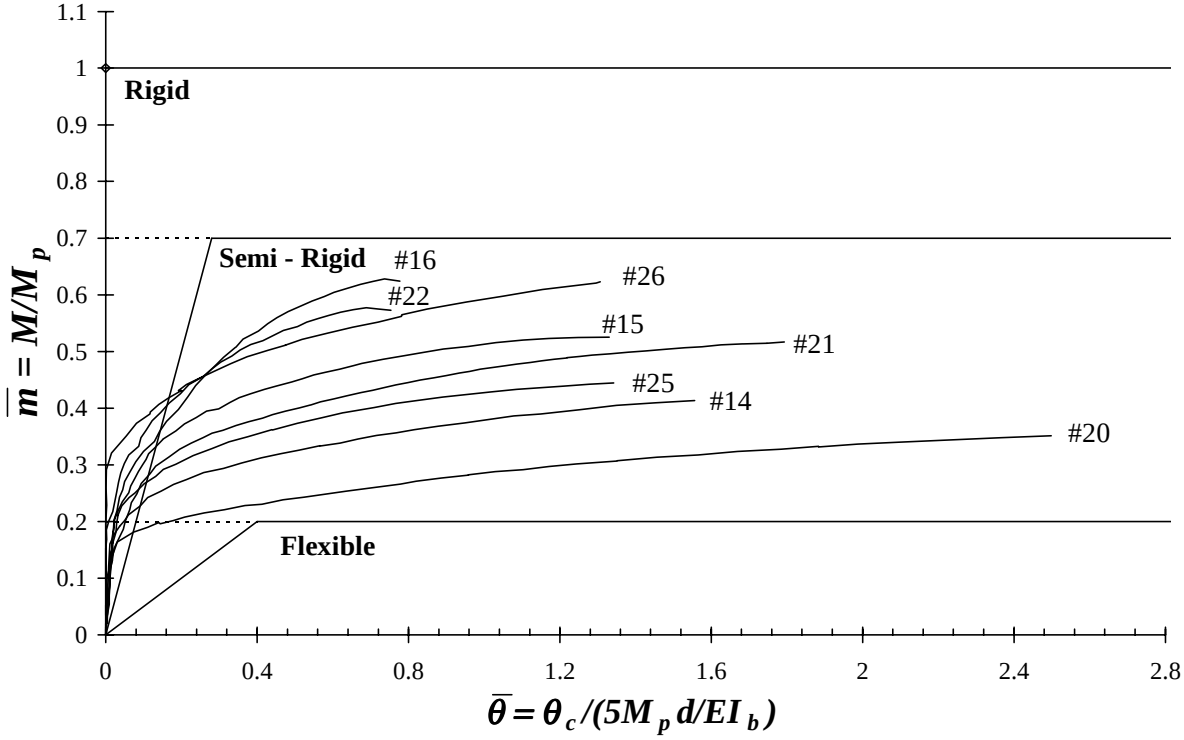

Figure 27 - Bjorhovde Classification -Type B, RHS

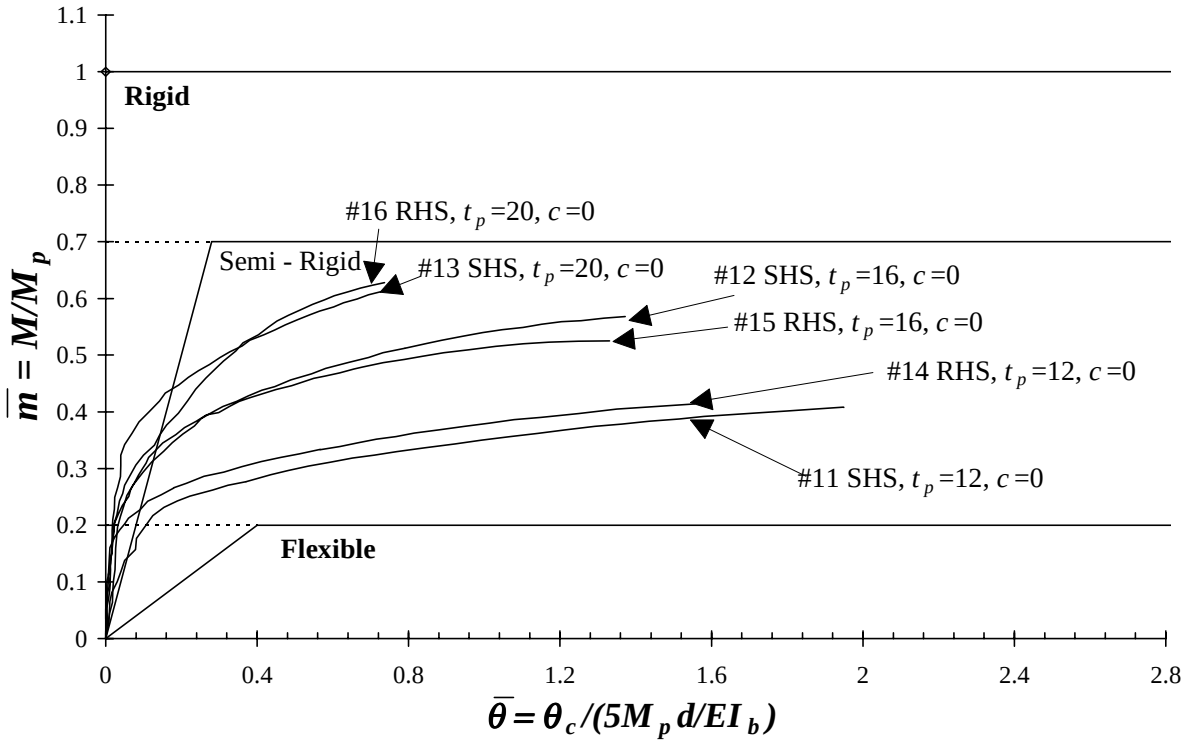

Figure 28 - Bjorhovde Classification Comparison

Table 1: Nominal Section Dimensions

Specimen No.	Section Geometry $d \times b \times t$	Shape	$\frac{b-2t}{t}$
1, 3-4, 7-8, 11-13, 17-19, 23, 24	$150 \times 150 \times 9$	SHS	14.7
2, 5-6, 9-10, 14-16, 20-22, 25, 26	$100 \times 200 \times 9$	RHS	9.11

Table 2: Flange Plate Dimensions

Specimen No.	Type	Section Shape	Plate Dimensions‡						Bolts	
			t_p	W_p	D_p	s_o	g	c	No.	l_B
1	A	SHS	16	280	280	35	30		8	75
2	A	RHS	16	230	330	35	15		8	75
3	A	SHS	12	280	280	35	30		8	75
4	A	SHS	20	280	280	35	30		8	90
5	A	RHS	12	230	330	35	15		8	75
6	A	RHS	20	230	330	35	15		8	90
7	A	SHS	16	260	260	25	30		8	75
8	A	SHS	16	300	300	45	30		8	75
9	A	RHS	16	210	310	25	30		8	75
10	A	RHS	16	250	350	45	30		8	75
11	B	SHS	12	210	280	35		0	4	75
12	B	SHS	16	210	280	35		0	4	75
13, 13*	B	SHS	20	210	280	35		0	4	90
14	B	RHS	12	160	330	35		0	4	75
15	B	RHS	16	160	330	35		0	4	75
16	B	RHS	20	160	330	35		0	4	90
17	B	SHS	12	280	280	35		35	4	75
18	B	SHS	16	280	280	35		35	4	75
19, 19*	B	SHS	20	280	280	35		35	4	90
20	B	RHS	12	230	330	35		35	4	75
21	B	RHS	16	230	330	35		35	4	75
22	B	RHS	20	230	330	35		35	4	90
23	B	SHS	16	210	260	45		0	4	75
24	B	SHS	16	210	300	25		0	4	75
25	B	RHS	16	160	310	45		0	4	75
26	B	RHS	16	160	350	25		0	4	75

‡ *a_e is equal to 30 mm for all specimens*

* *see note Table 5*

Table 3: Result of Tensile Coupon Tests - Sections

Section[+]	Position	f_y (MPa)	f_u (MPa)	f_u/f_y	f_y/f_{yn}	f_u/f_{un}	e_u (%)
SHS1	Opposite	418	442	1.06	1.19	0.98	10.8
	Adjacent	419	449	1.07	1.20	1.00	13.1
	Corner	498	550	1.10	1.42	1.22	1.4
SHS2	Opposite	425	459	1.08	1.21	1.02	8.1
	Adjacent	404	441	1.09	1.15	0.98	12.5
	Corner	467	511	1.09	1.33	1.14	1.7
SHS3	Opposite	419	453	1.08	1.20	1.01	14.9
	Adjacent	399	445	1.12	1.14	0.99	15.7
	Corner	497	540	1.09	1.42	1.20	1.8
SHS4	Opposite	410	432	1.05	1.17	0.96	9.8
	Adjacent	398	430	1.08	1.14	0.96	10.2
	Corner	499	535	1.07	1.43	1.19	2.0
RHS1	Opposite	407	458	1.13	1.16	1.02	12.8
	Adjacent	378	440	1.16	1.08	0.98	12.6
	Corner	461	511	1.11	1.32	1.14	2.2
RHS2	Opposite	408	452	1.11	1.17	1.00	13.6
	Adjacent	378	446	1.18	1.08	0.99	13.2
	Corner	444	482	1.09	1.27	1.07	1.6

[+] *No coupons taken from sections SHS5, RHS3 and RHS4*

Note:
f_{yn} = 350 MPa
f_{un} = 430 MPa

Opposite *taken from the face opposite the seam weld*
Adjacent *taken from face adjacent to seam weld*
Corner *taken from corner of section*

Table 4: Result of Tensile Coupon Tests - Plates

Plate Thickness (mm)	f_y (MPa)	f_u (MPa)	f_u/f_y	f_y/f_{yn}	f_u/f_{un}	e_u (%)
12	354	499	1.41	1.01	1.11	20.3
16	349	482	1.38	1.00	1.07	20.6
20	351	496	1.41	1.00	1.11	22.0

Note:
f_{yn} = 350 MPa
f_{un} = 450 MPa

Table 5 - Ultimate Moment and Rotation Results

Specimen #	Specimen Section	Ultimate Moment M_u (kN.m)	Ultimate Rotation θ_{cu} (rad)	M_u/M_n	M_u/M_p	Mode at Ultimate†
1	SHS2	116.0	0.068	1.33	0.97	Bolt
2	RHS2	124.5	0.037	1.22	0.90	Punching
3	SHS2	93.9	0.087	1.08	0.79	Bolt
4	SHS2	116.0	0.013	1.33	0.97	Bolt
5	RHS2	92.7	0.023	0.91	0.67	Punching
6	RHS2	136.7	0.009	1.34	0.99	Bolt
7	SHS5	106.0	0.017	1.22	0.89	Bolt
8	SHS1	97.6	0.039	1.12	0.82	Punching
9	RHS1	133.0	0.018	1.30	0.96	Punching
10	RHS2	119.3	0.039	1.17	0.86	Punching
11	SHS3	48.6	0.056	0.56	0.41	Deformation
12	SHS3	69.0	0.049	0.79	0.58	Bolt
13*	SHS3	70.3	0.024	0.81	0.59	Bolt Thread
13	SHS5	77.4	0.034	0.89	0.65	Bolt
14	RHS3	57.1	0.045	0.56	0.41	Deformation
15	RHS3	72.5	0.039	0.71	0.53	Bolt
16	RHS4	86.6	0.021	0.85	0.63	Bolt
17	SHS3	38.6	0.069	0.44	0.32	Deformation
18	SHS4	59.5	0.061	0.68	0.50	Bolt
19*	SHS4	67.8	0.030	0.78	0.57	Bolt Thread
19	SHS5	72.4	0.059	0.83	0.61	Bolt
20	RHS3	48.5	0.076	0.48	0.35	Deformation
21	RHS4	71.3	0.054	0.70	0.52	Bolt
22	RHS3	79.6	0.021	0.78	0.58	Bolt
23	SHS4	58.3	0.060	0.67	0.49	Bolt
24	SHS4	66.6	0.037	0.77	0.56	Bolt
25	SHS4	62.1	0.047	0.61	0.45	Bolt
26	SHS1	86.0	0.041	0.84	0.62	Bolt

Note:

SHS M_p **= 119 kN.m** M_n **= 87 kN.m**

RHS M_p **= 138 kN.m** M_n **= 102 kN.m**

† **Bolt** = *failure by bolt fracture*
Bolt Thread = *failure by stripping of bolt threads*
Punching = *failure by section tearing away from plate at to of weld (punching shear)*
Deformation = *test terminated due to excessive deflections.*

* *denotes repeated tests, Metric Grade 8.8 bolts used in test as apposed to Structural Grade 8.8 bolts*

Appendix A - *Test Results*

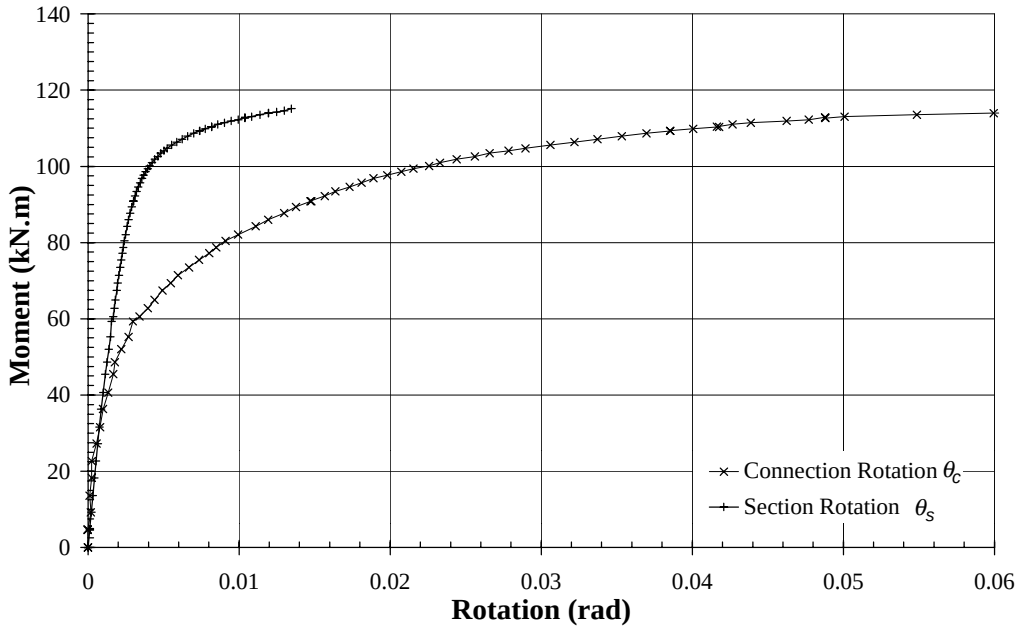

FIG A1: APPLIED BENDING MOMENT VS. CONNECTION ROTATION for Test #1 - SHS, t_p=16 mm, s_o=35 mm

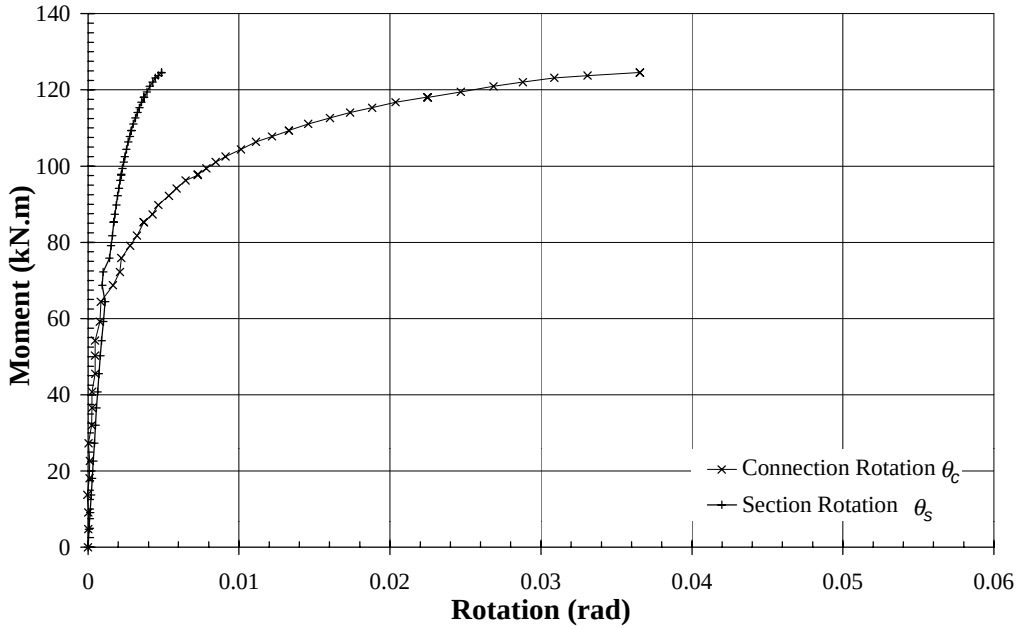

FIG A2: APPLIED BENDING MOMENT VS. CONNECTION ROTATION for Test #2 - RHS, t_p=16 mm, s_o=35 mm

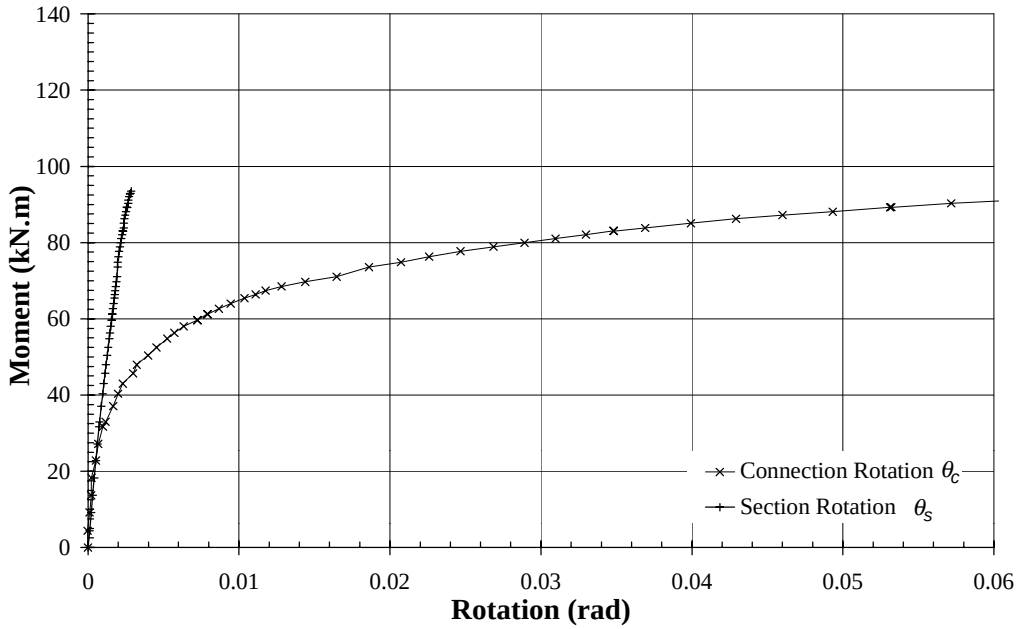

FIG A3: APPLIED BENDING MOMENT VS. CONNECTION ROTATION for Test #3 - SHS, t_p=12 mm, s_o=35 mm

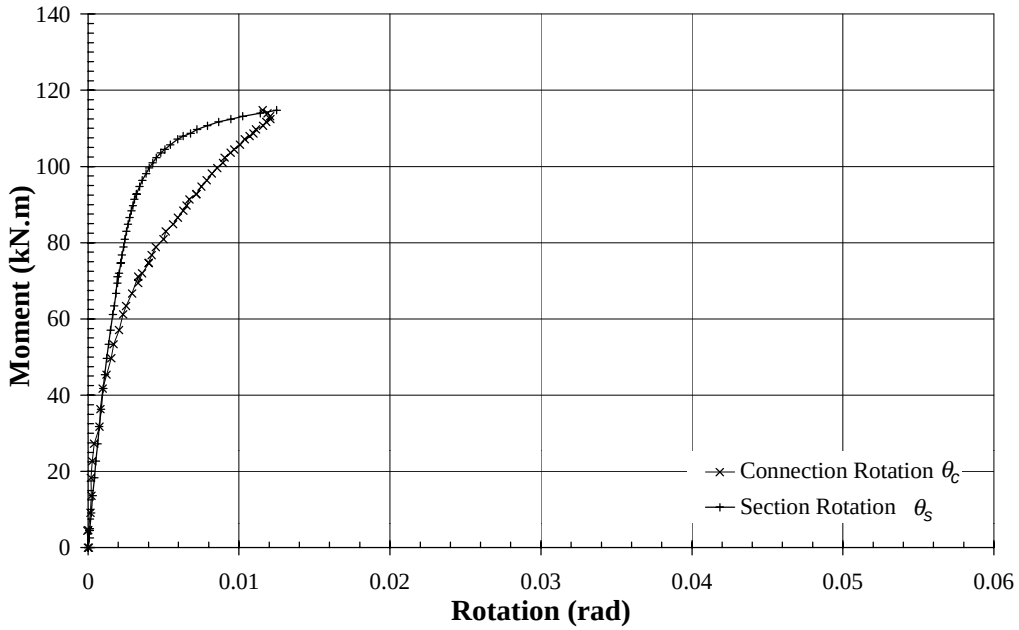

FIG A4: APPLIED BENDING MOMENT VS. CONNECTION ROTATION for Test #4 - SHS, t_p=20 mm, s_o=35 mm

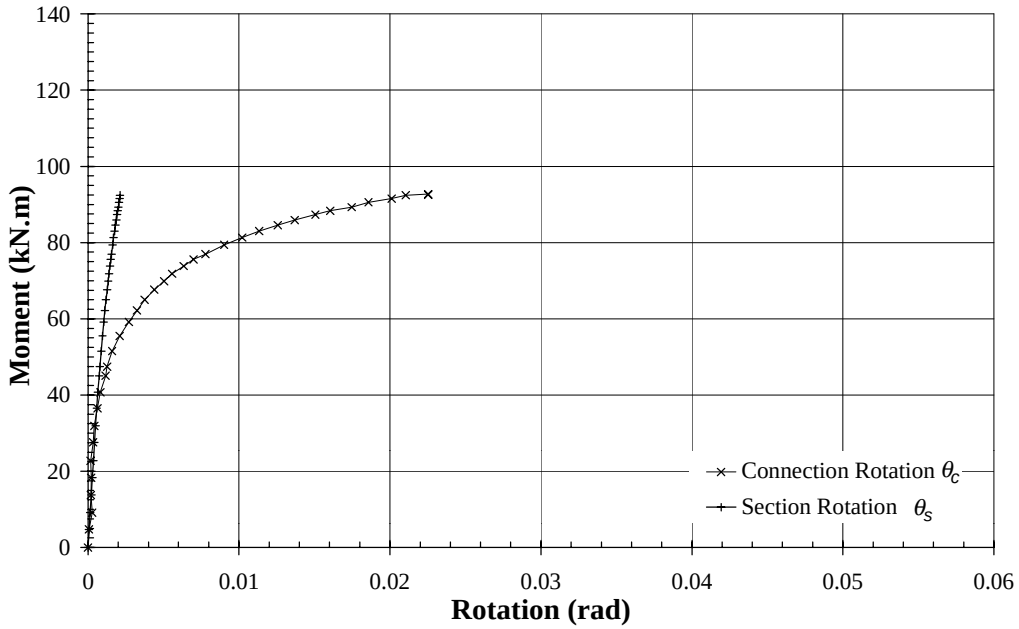

FIG A5: APPLIED BENDING MOMENT VS. CONNECTION ROTATION for Test #5 - RHS, t_p=12 mm, s_o=35 mm

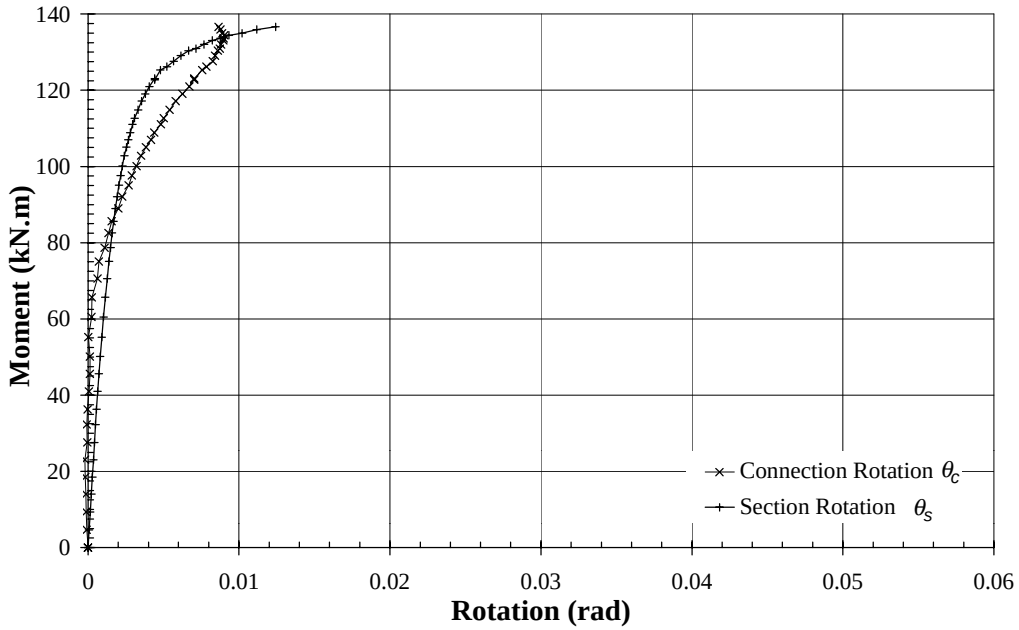

FIG A6: APPLIED BENDING MOMENT VS. CONNECTION ROTATION for Test #6 - RHS, t_p=20 mm, s_o=35 mm

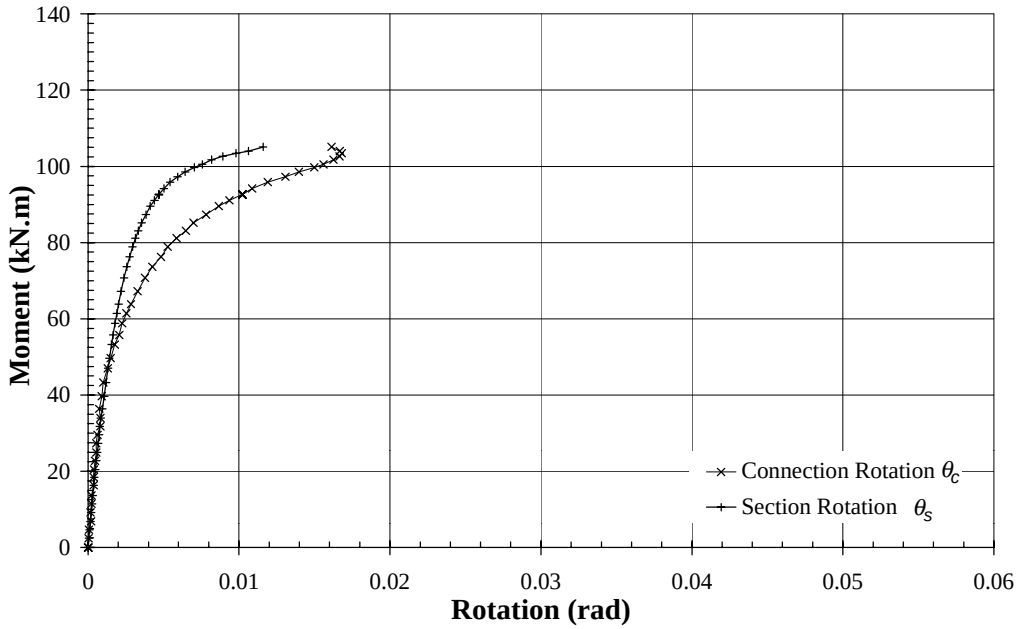

FIG A7: APPLIED BENDING MOMENT VS. CONNECTION ROTATION for Test #7 - SHS, t_p=16 mm, s_o=25 mm

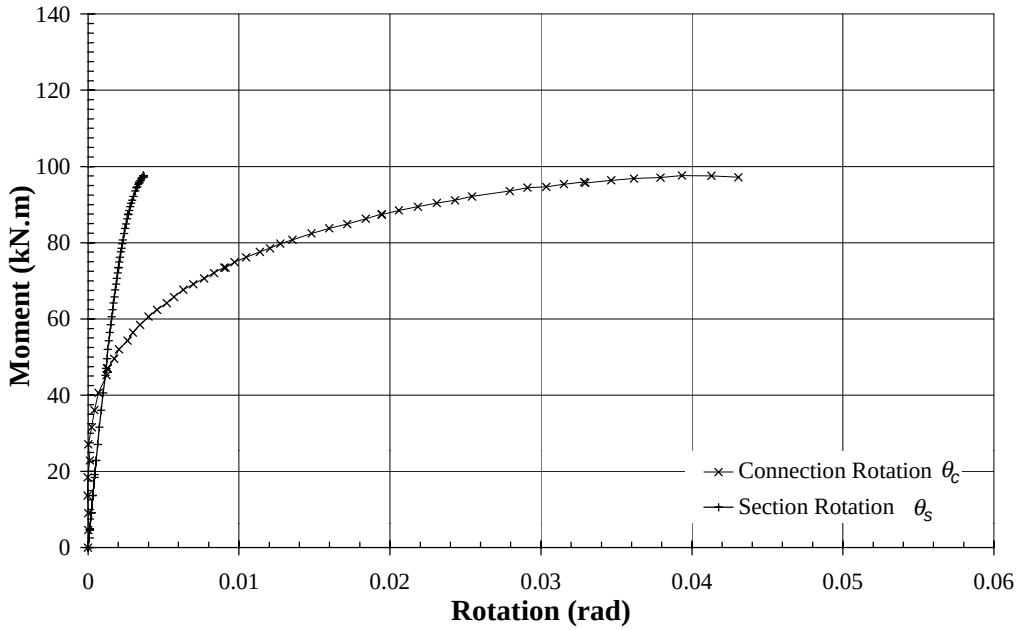

FIG A8: APPLIED BENDING MOMENT VS. CONNECTION ROTATION for Test #8 - SHS, t_p=16 mm, s_o=45 mm

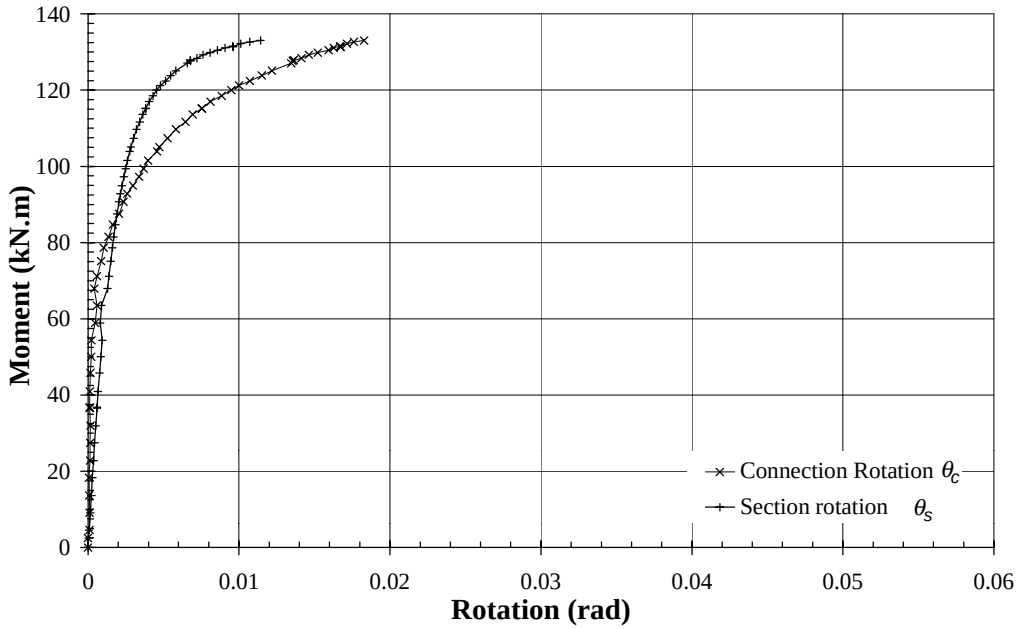

FIG A9: APPLIED BENDING MOMENT VS. CONNECTION ROTATION for Test #9 - RHS, t_p=16 mm, s_o=25 mm

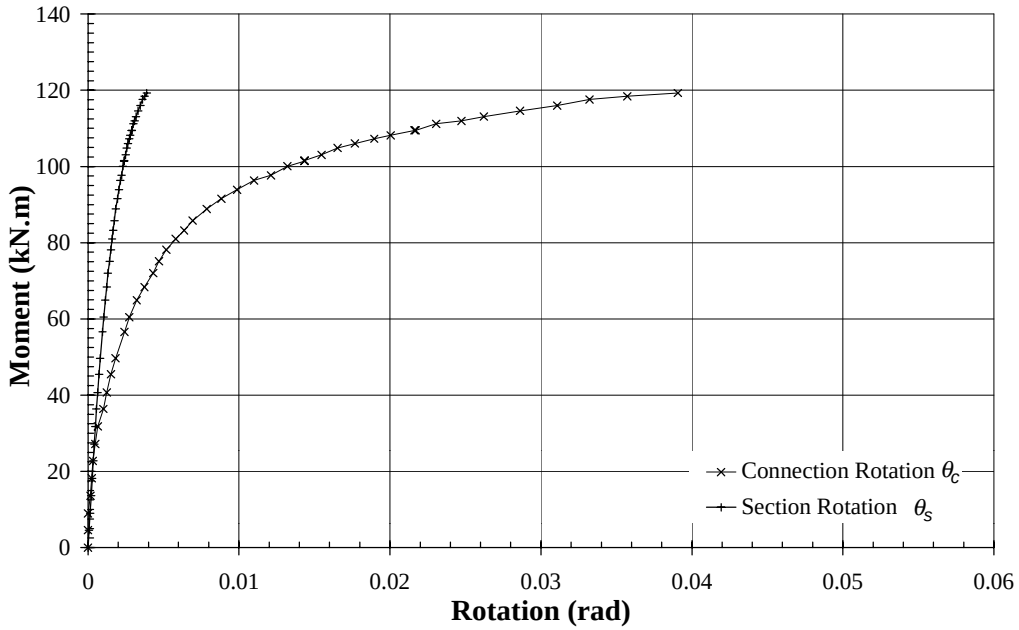

FIG A10: APPLIED BENDING MOMENT VS. CONNECTION ROTATION for Test #10 - RHS, t_p=16 mm, s_o=45 mm

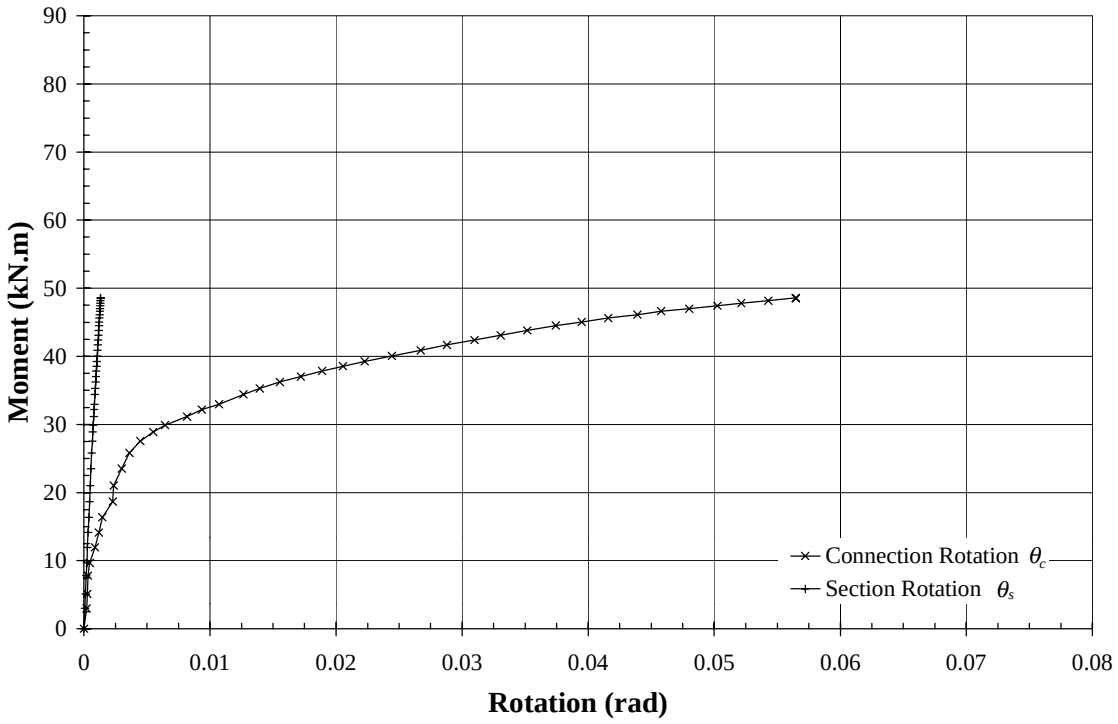

FIG A11: APPLIED BENDING MOMENT VS. CONNECTION ROTATION for Test #11 - SHS, Type B, t_p=12 mm, c=0 mm

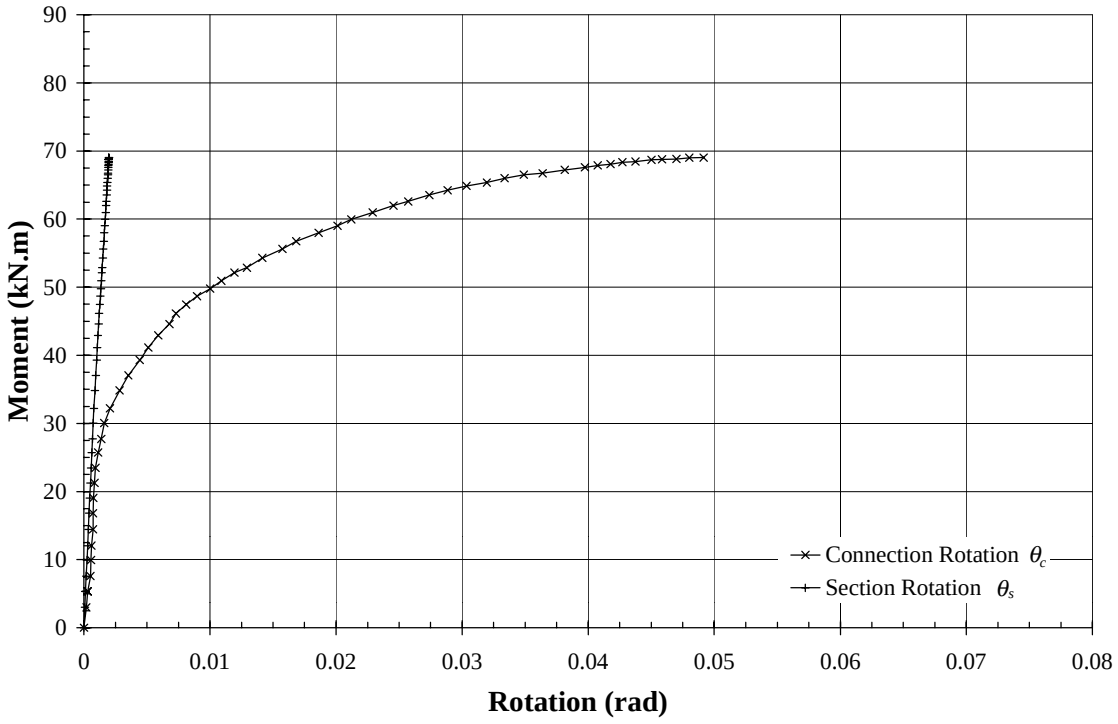

FIG A12: APPLIED BENDING MOMENT VS. CONNECTION ROTATION for Test #12 - SHS, Type B, t_p=16 mm, c=0 mm

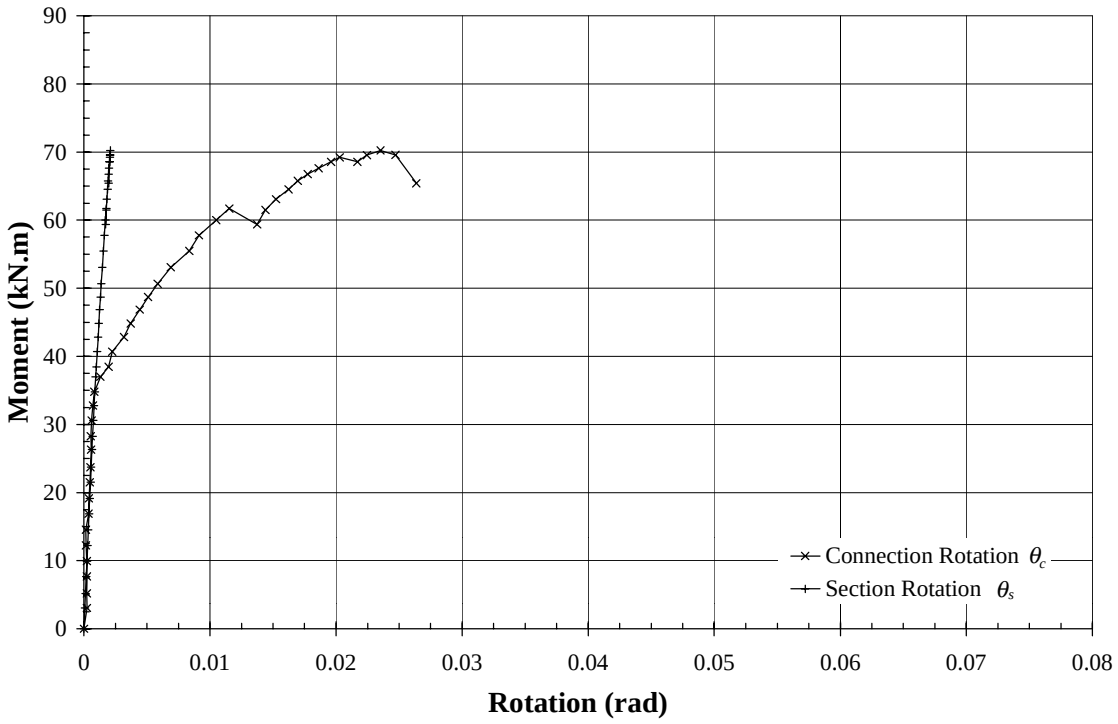

FIG A13: APPLIED BENDING MOMENT VS. CONNECTION ROTATION for Test #13* - SHS, Type B, t_p=20 mm, c=0 mm

(Metric Grade 8.8 Bolts used in test 13, Structural Grade 8.8 Bolts used in test 13)*

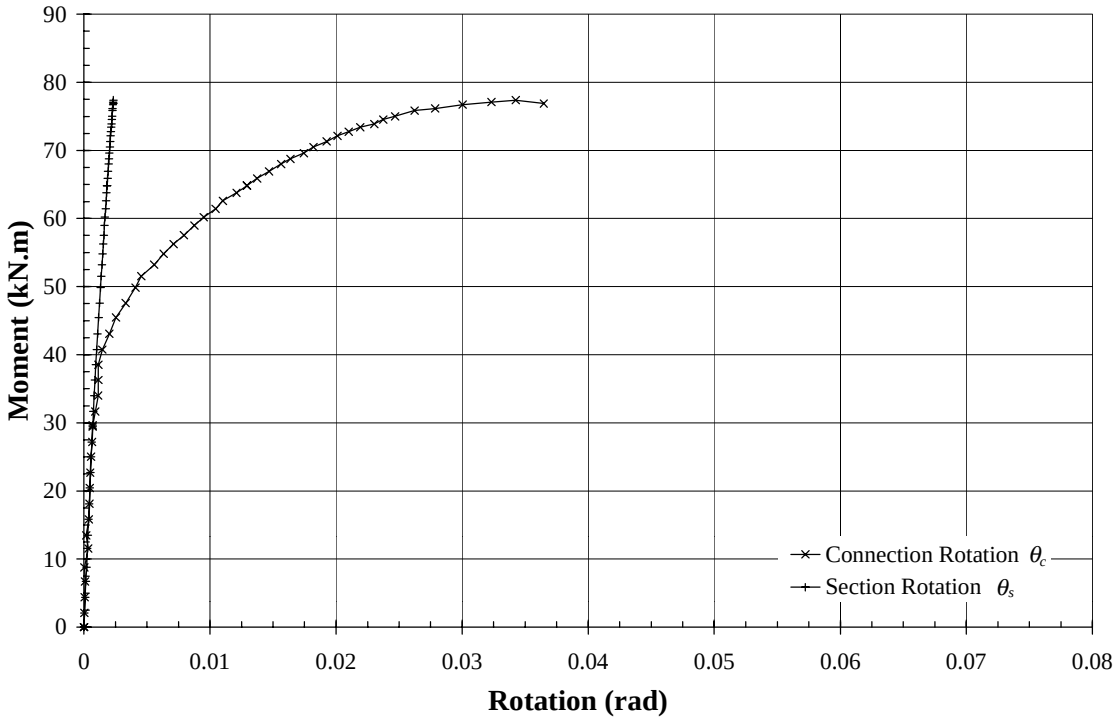

FIG A14: APPLIED BENDING MOMENT VS. CONNECTION ROTATION for Test #13 - SHS, Type B, t_p=20 mm, c=0 mm

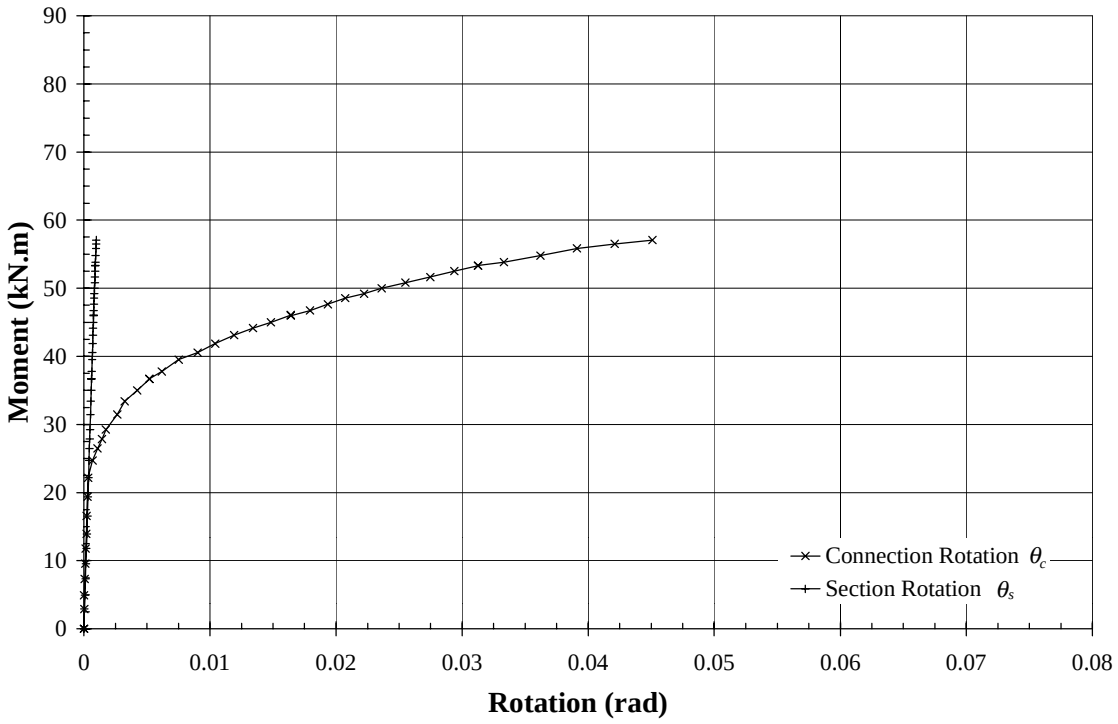

FIG A15: APPLIED BENDING MOMENT VS. CONNECTION ROTATION for Test #14 - RHS, Type B, t_p=12 mm, c=0 mm

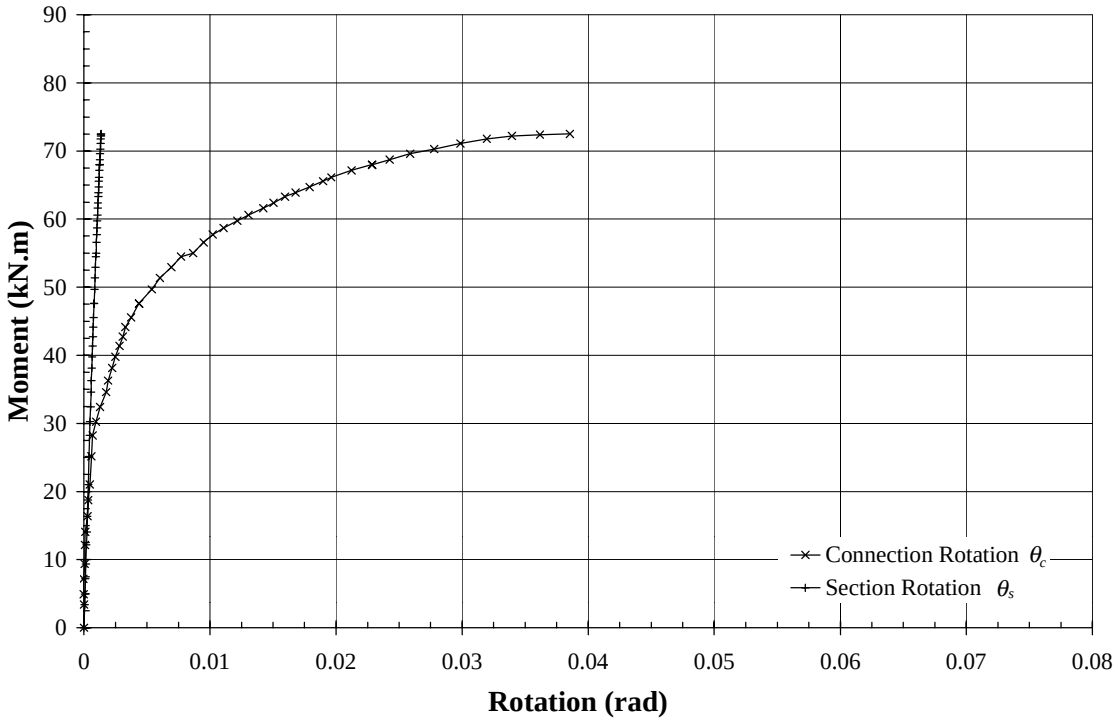

FIG A16: APPLIED BENDING MOMENT VS. CONNECTION ROTATION for Test #15 - RHS, Type B, t_p=16 mm, c=0 mm

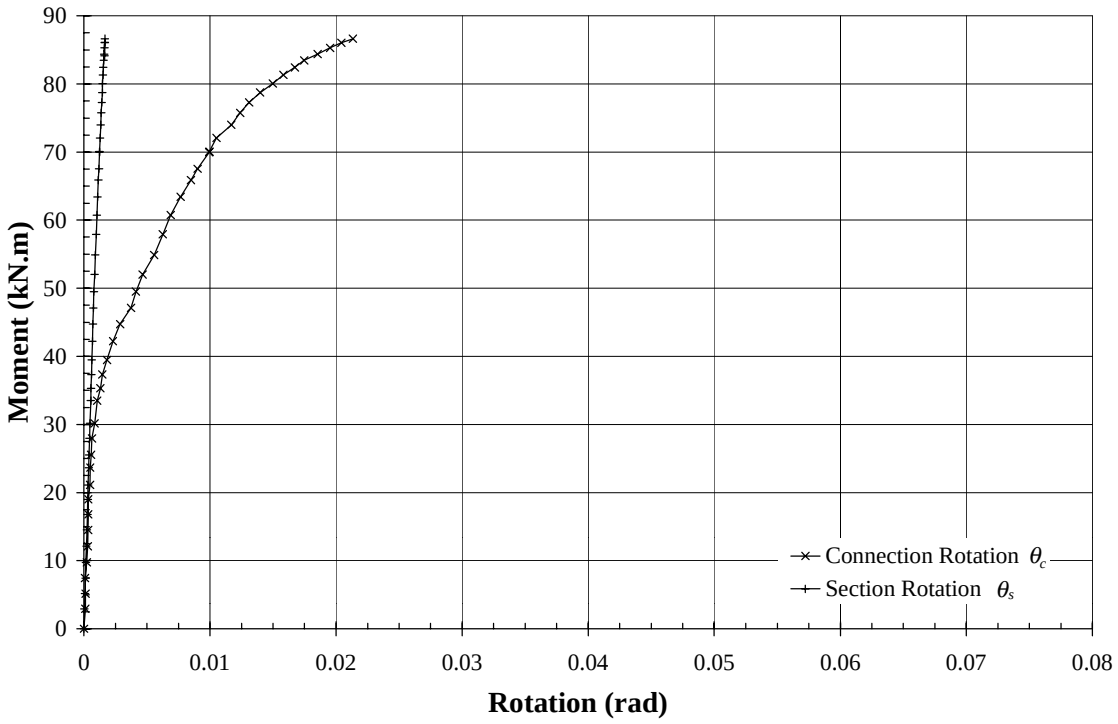

FIG A17: APPLIED BENDING MOMENT VS. CONNECTION ROTATION for Test #16 - RHS, Type B, t_p=20 mm, c=0 mm

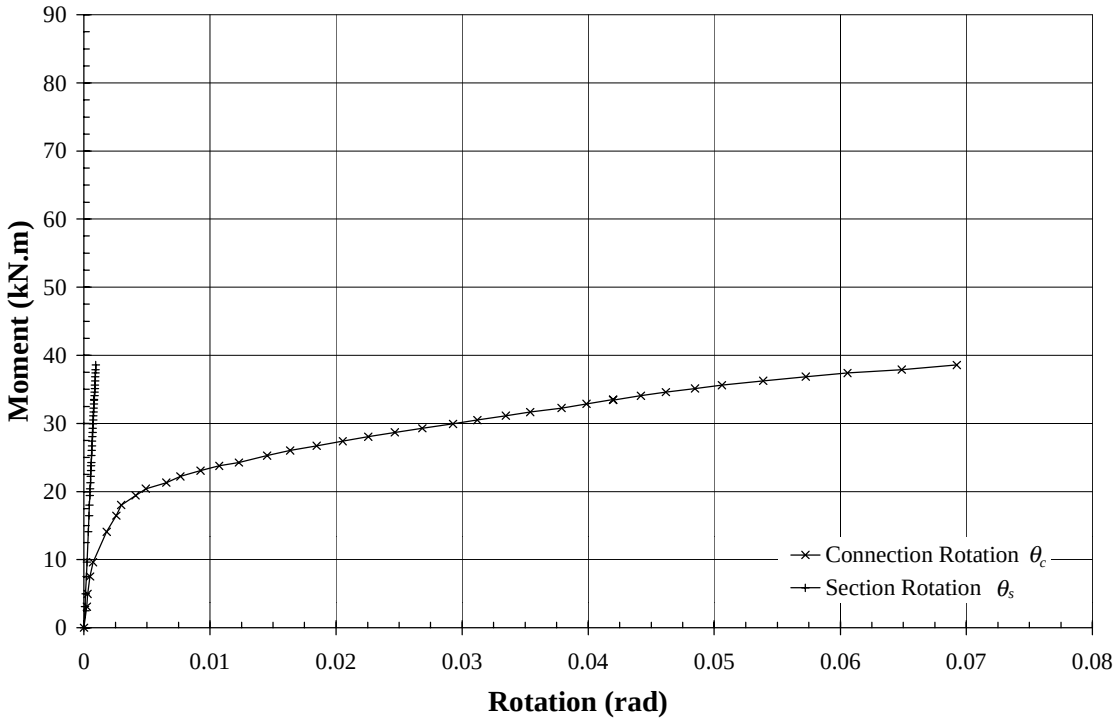

FIG A18: APPLIED BENDING MOMENT VS. CONNECTION ROTATION for Test #17 - SHS, Type B, t_p=12 mm, c=30 mm

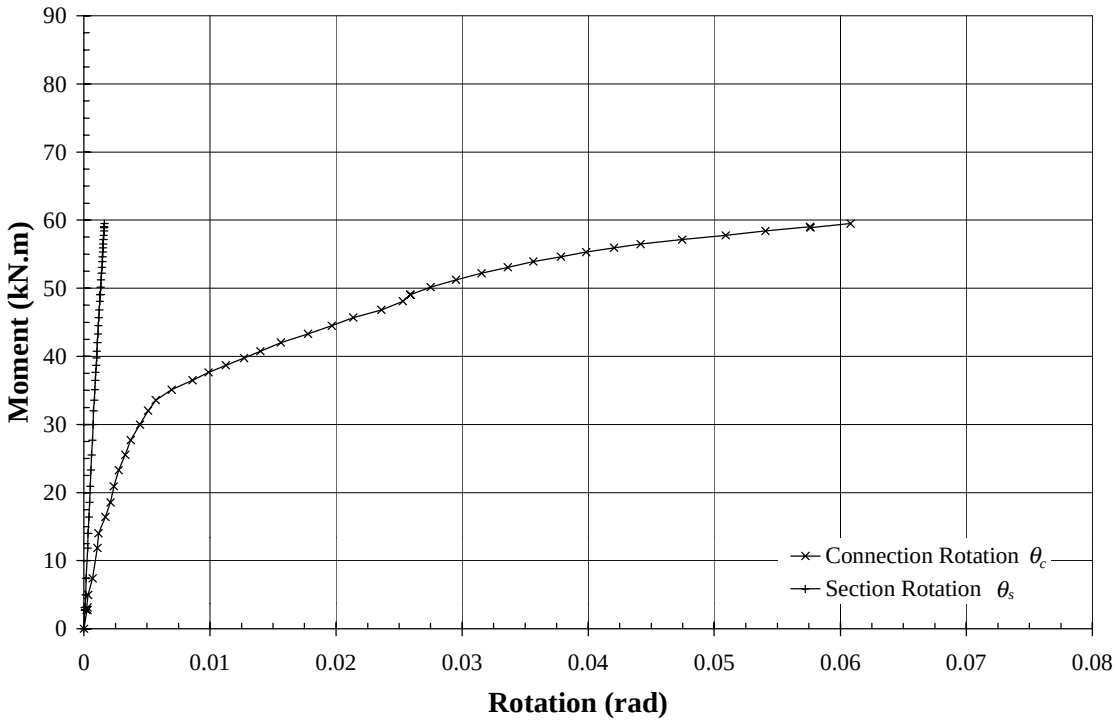

FIG A19: APPLIED BENDING MOMENT VS. CONNECTION ROTATION for Test #18 - SHS, Type B, t_p=16 mm, c=30 mm

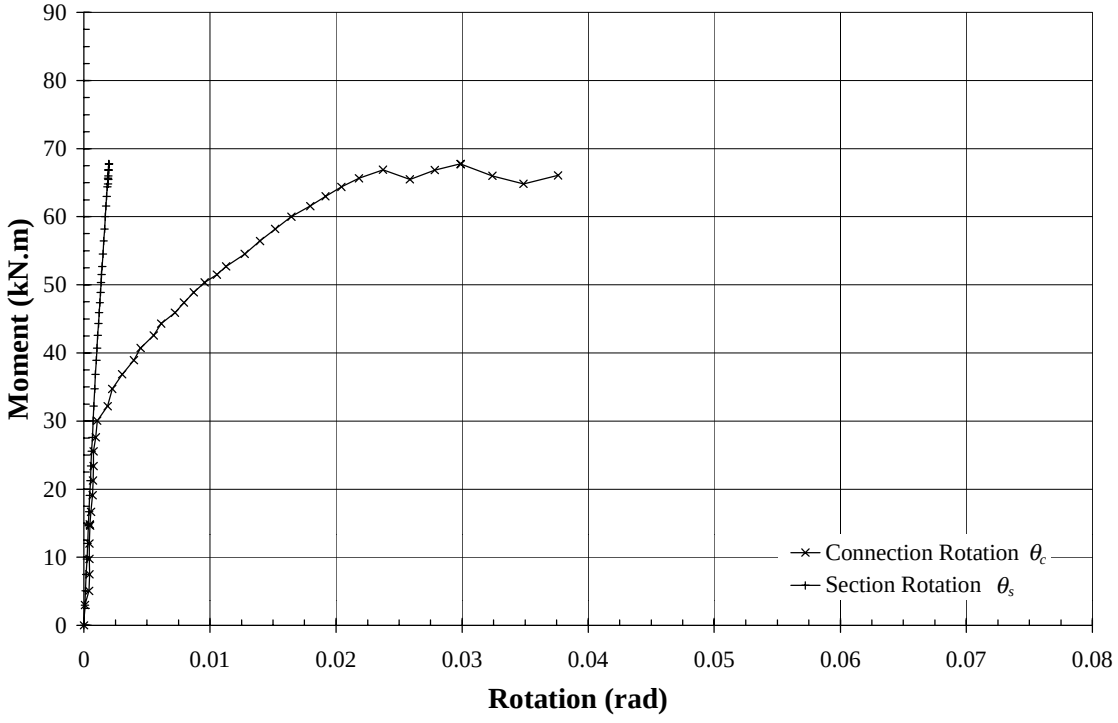

FIG A20: APPLIED BENDING MOMENT VS. CONNECTION ROTATION for Test #19* - SHS, Type B, t_p=20 mm, c=30 mm

(Metric Grade 8.8 Bolts used in test 19, Structural Grade 8.8 Bolts used in test 19)*

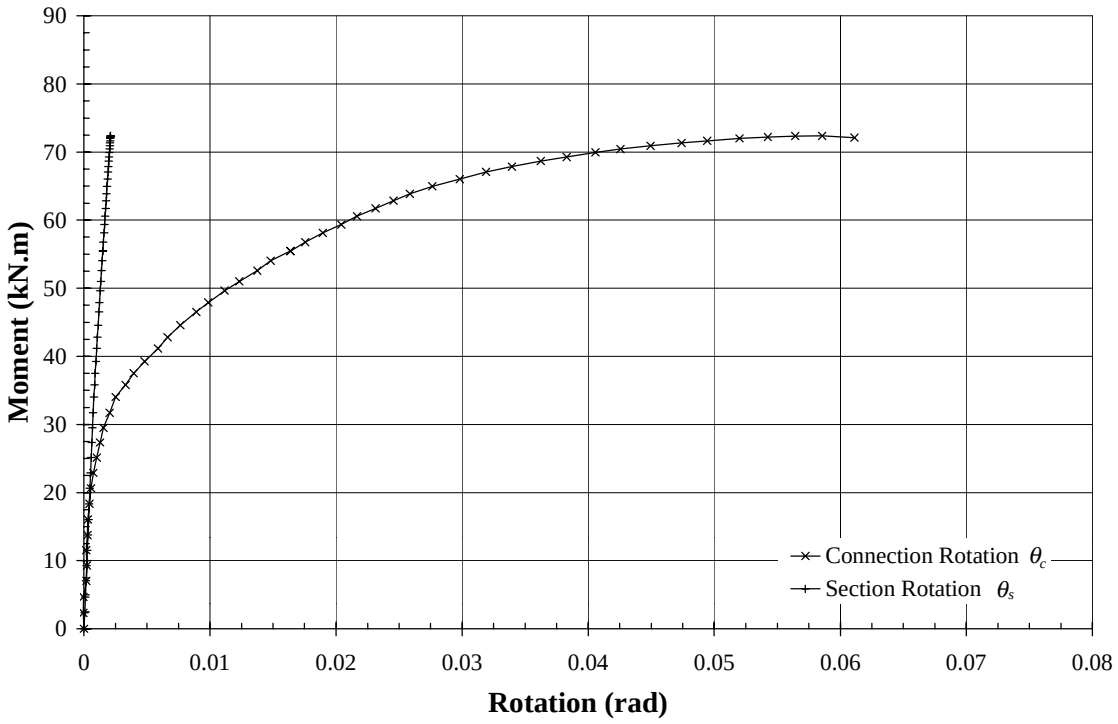

FIG A21: APPLIED BENDING MOMENT VS. CONNECTION ROTATION for Test #19 - SHS, Type B, t_p=20 mm, c=30 mm

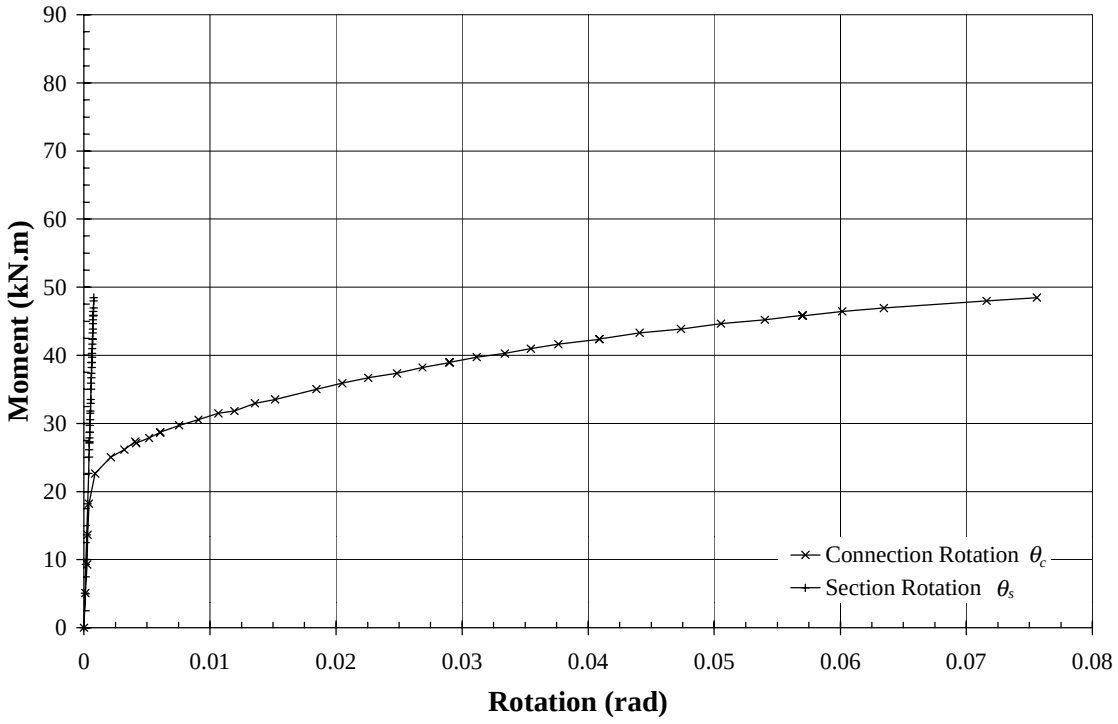

FIG A22: APPLIED BENDING MOMENT VS. CONNECTION ROTATION for Test #20 - RHS, Type B, t_p=12 mm, c=30 mm

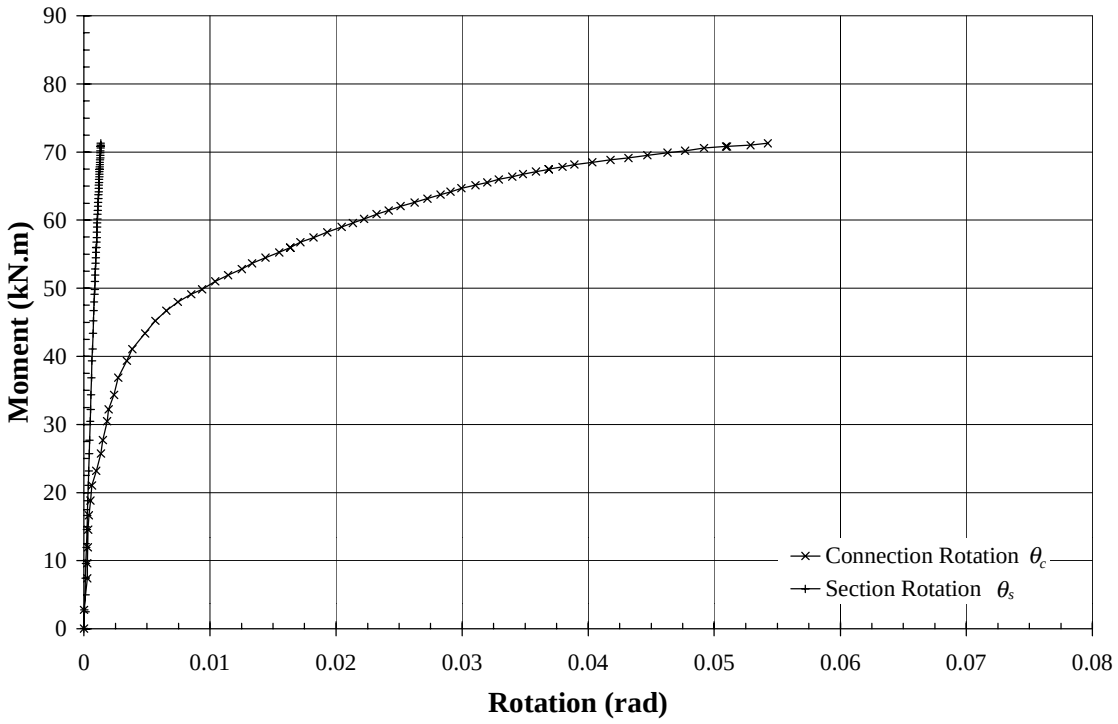

FIG A23: APPLIED BENDING MOMENT VS. CONNECTION ROTATION for Test #21 - RHS, Type B, t_p=16 mm, c=30 mm

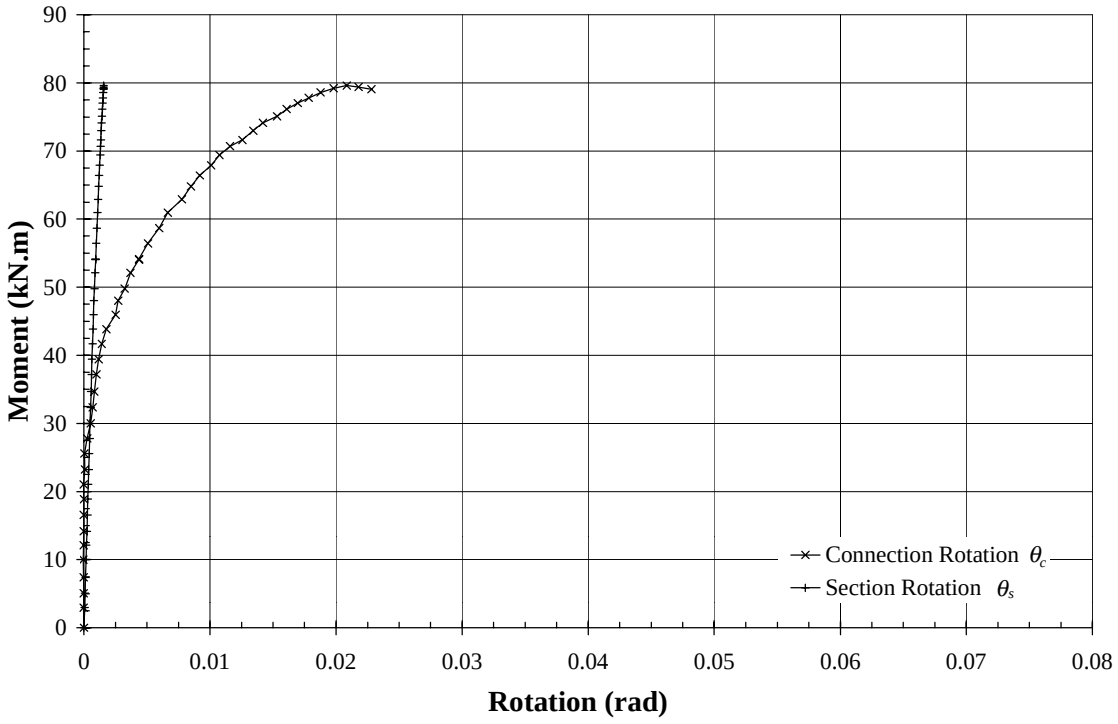

FIG A24: APPLIED BENDING MOMENT VS. CONNECTION ROTATION for Test #22 - RHS, Type B, t_p=20 mm, c=30 mm

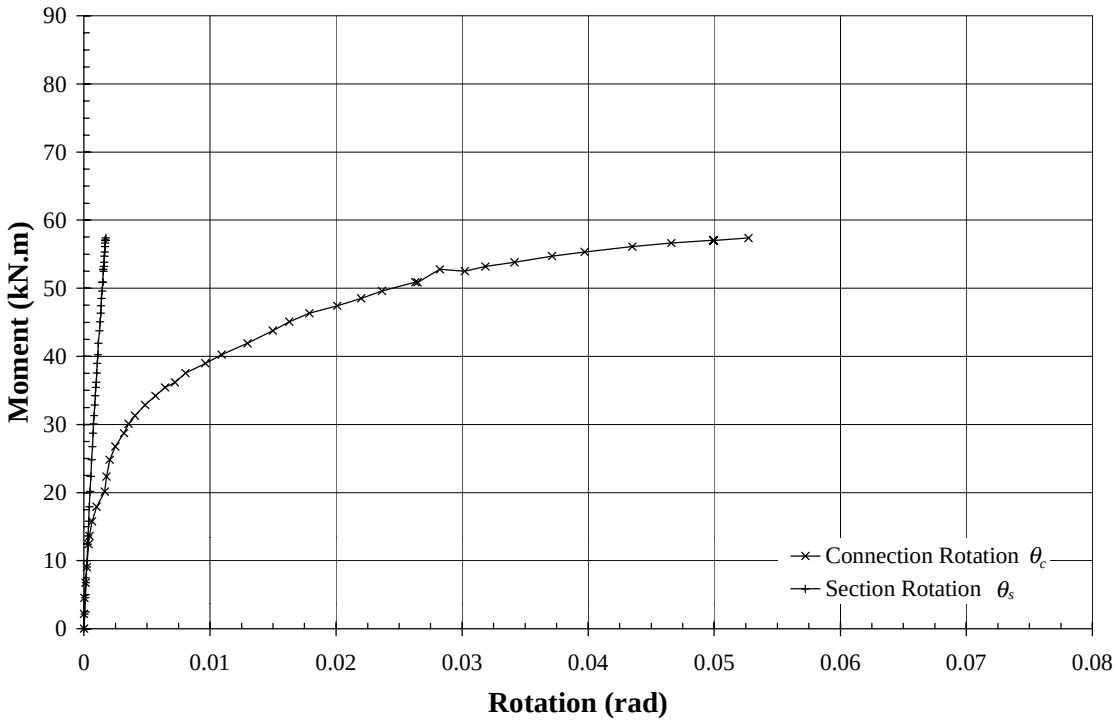

FIG A25: APPLIED BENDING MOMENT VS. CONNECTION ROTATION for Test #23 - SHS, Type B, t_p=16 mm, s_o=45 mm, c=0 mm

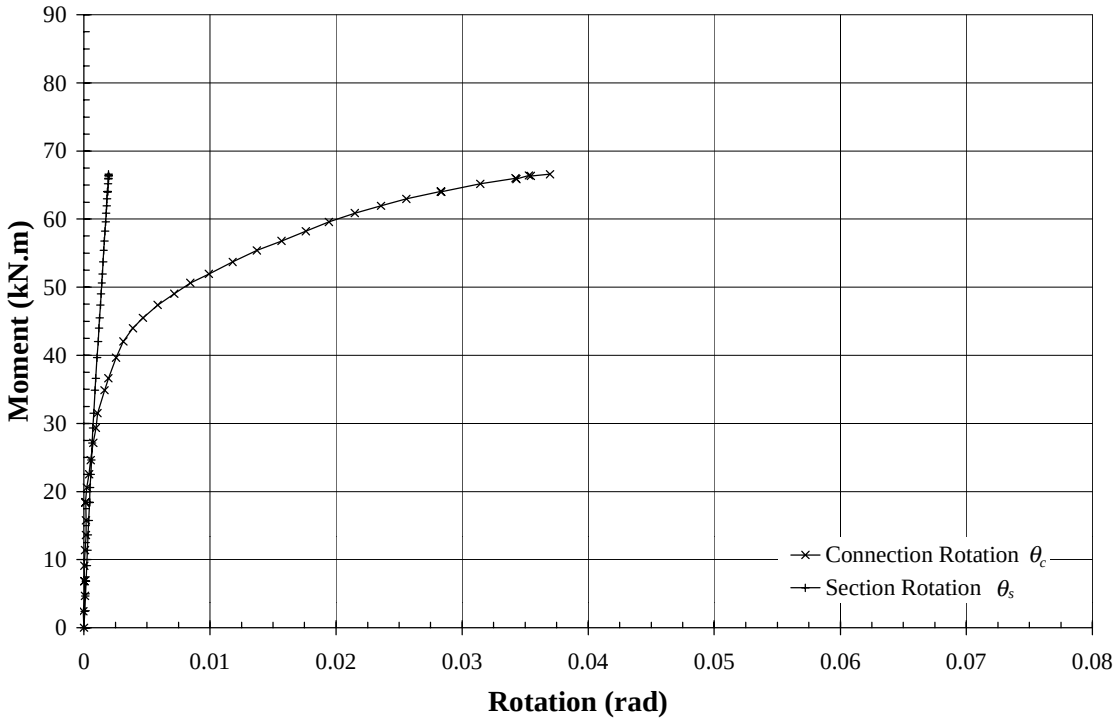

FIG A26: APPLIED BENDING MOMENT VS. CONNECTION ROTATION for Test #24 - SHS, Type B, t_p=16 mm, s_o=45 mm, c=0 mm

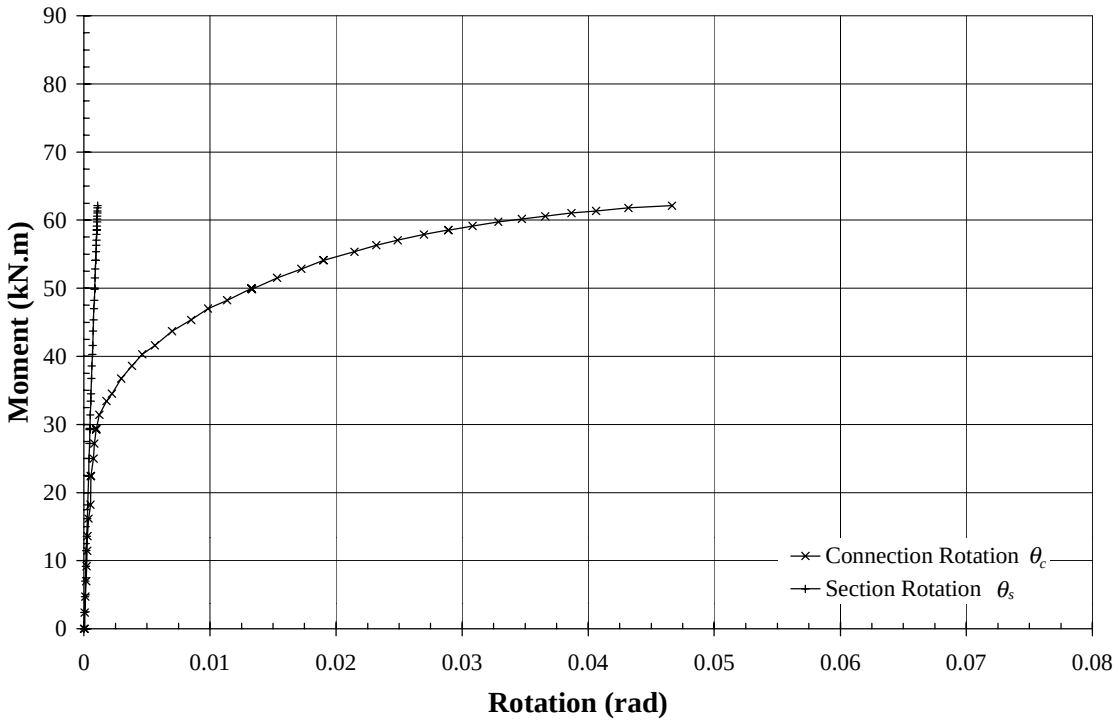

FIG A27: APPLIED BENDING MOMENT VS. CONNECTION ROTATION for Test #25 - RHS, Type B, t_p=16 mm, s_o=25 mm, c=0 mm

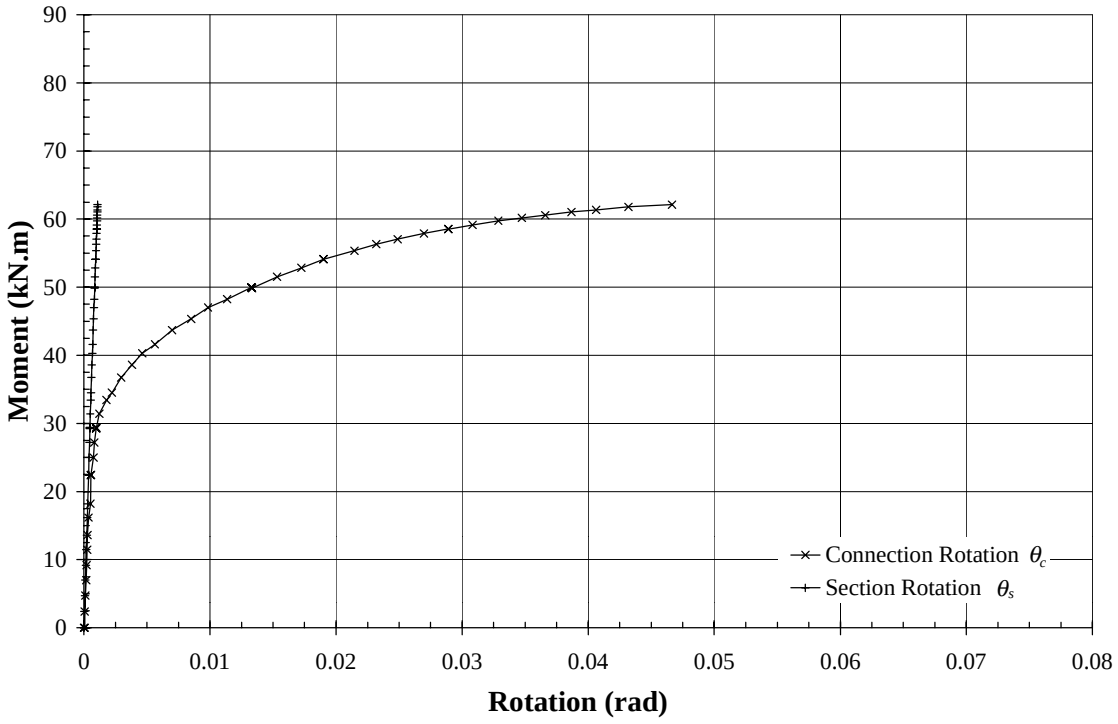

FIG A28: APPLIED BENDING MOMENT VS. CONNECTION ROTATION for Test #26 - RHS, Type B, t_p=16 mm, s_o=45 mm, c=0 mm

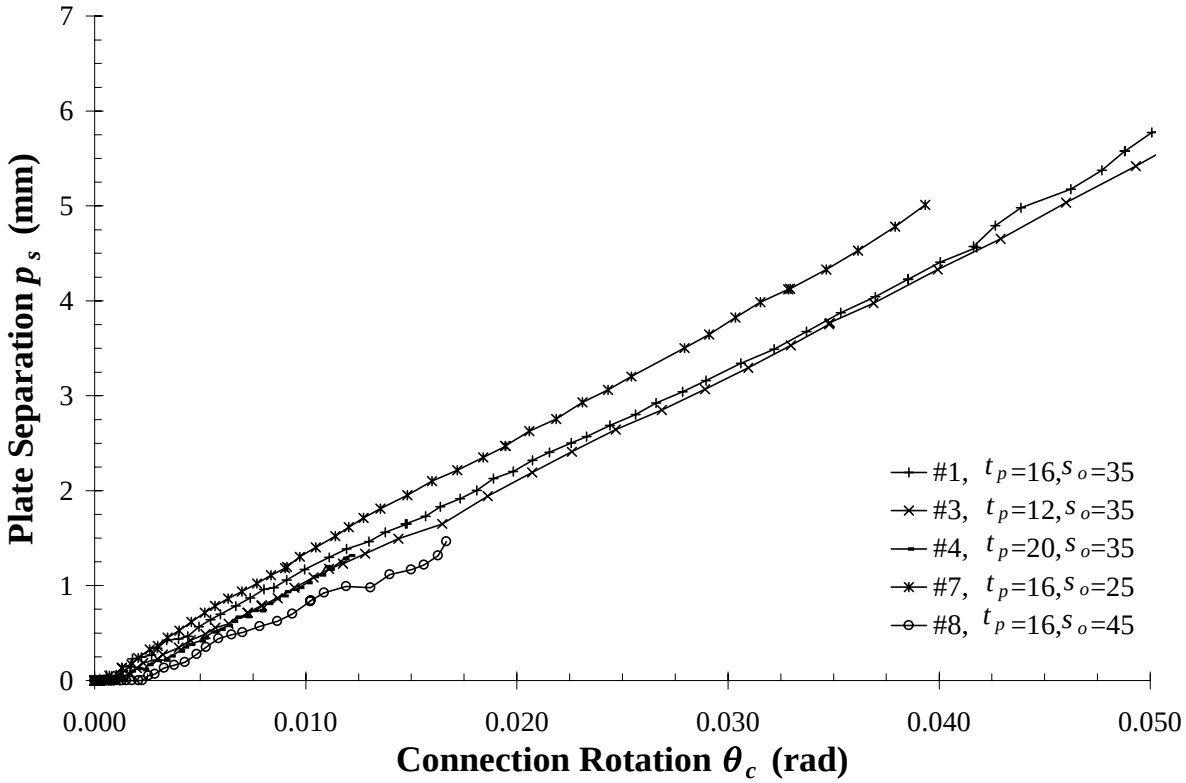

FIG A29: CONNECTION ROTATION VS. PLATE SEPARATION for Type A Connections - Square Hollow Sections

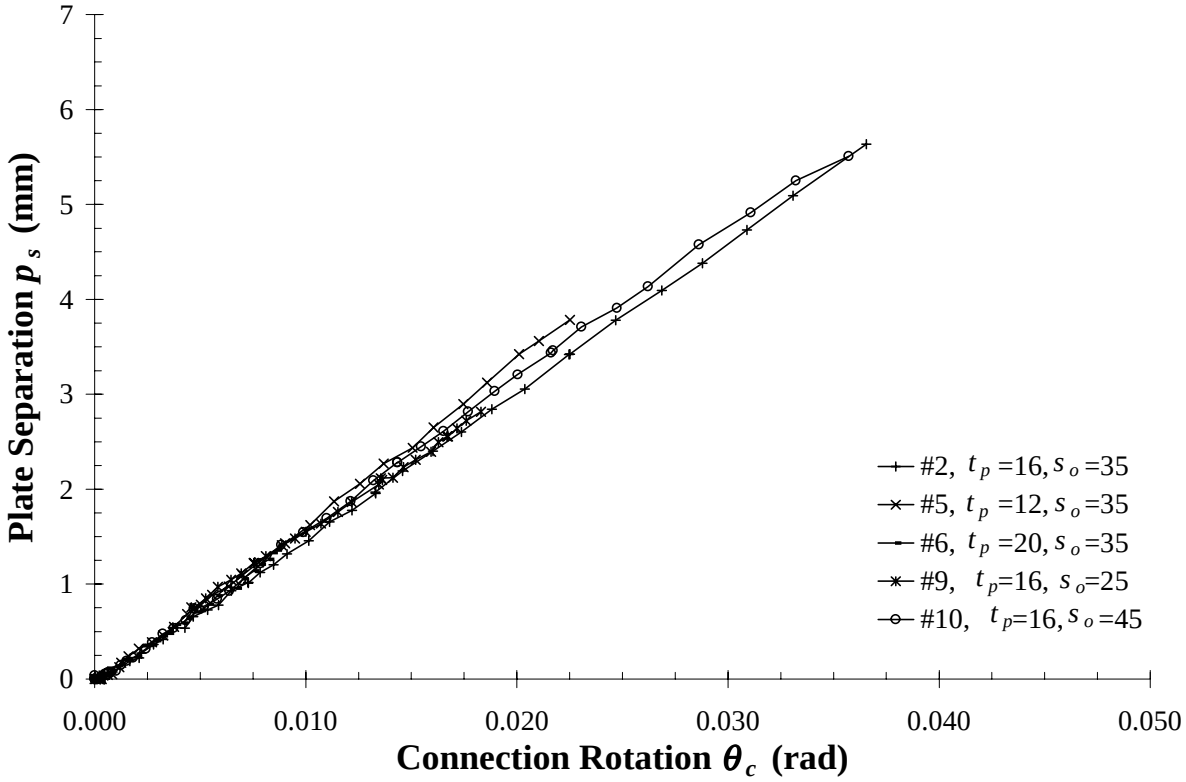

FIG A30: CONNECTION ROTATION VS. PLATE SEPARATION for Type A Connections - Rectangular Hollow Sections

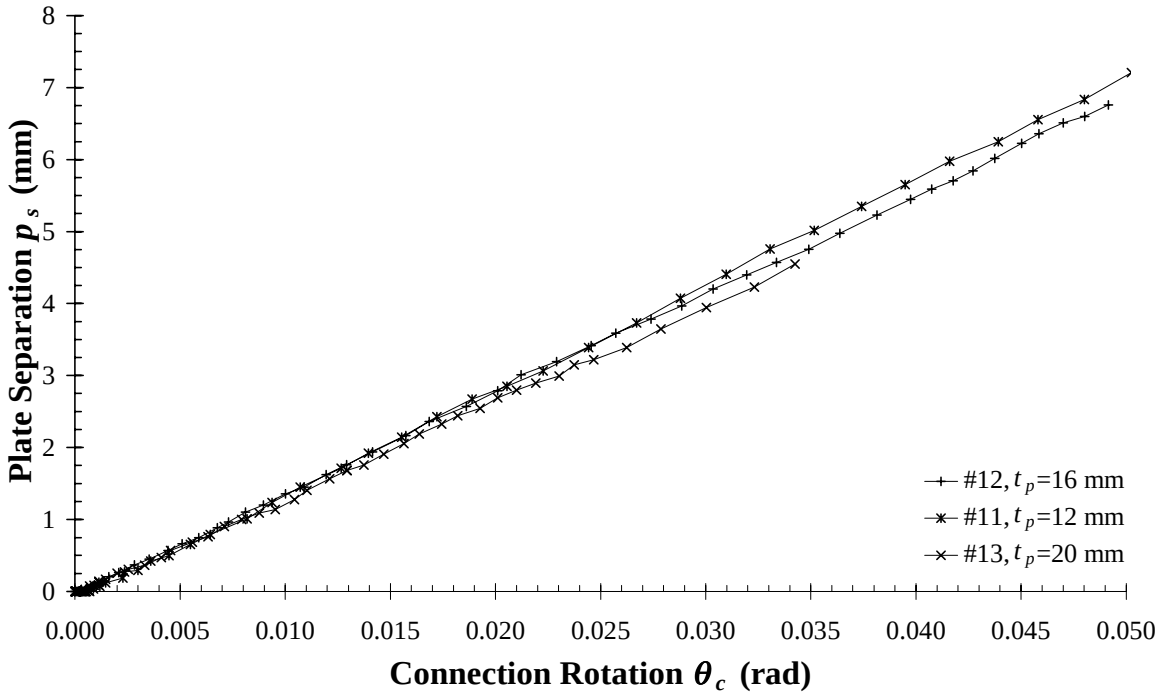

FIG A31: CONNECTION ROTATION VS. PLATE SEPARATION for Type B Connections- Square Hollow Sections, W_p=210mm

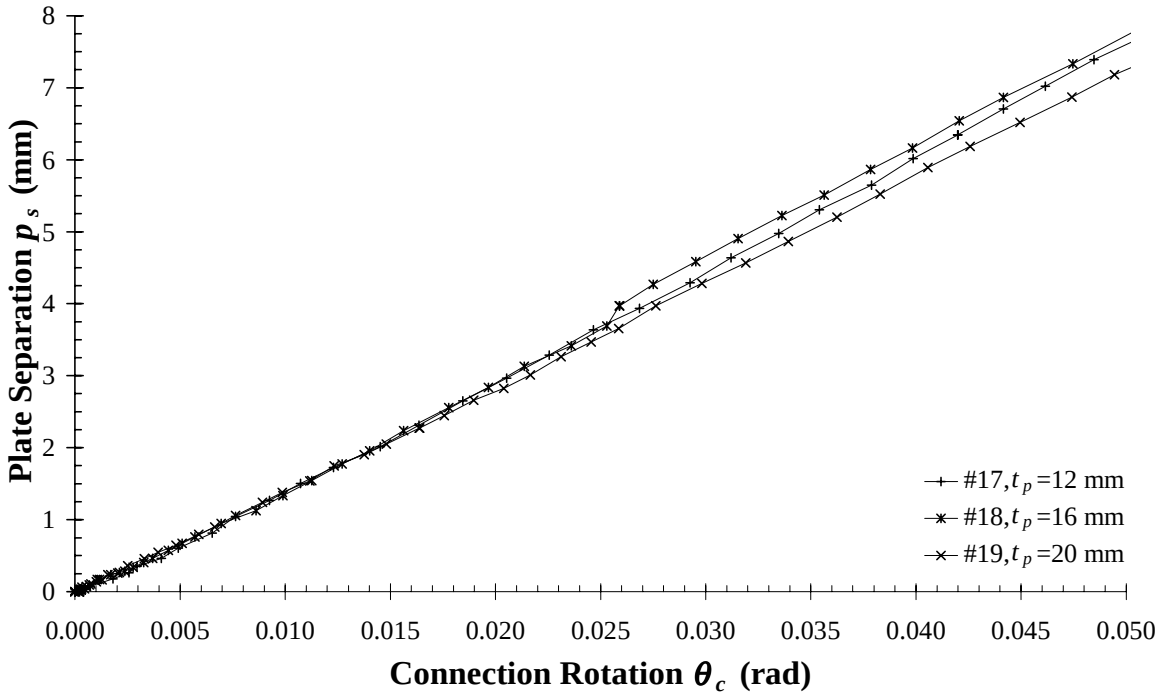

FIG A32: CONNECTION ROTATION VS. PLATE SEPARATION for Type B Connections - Square Hollow Sections, W_p=280mm

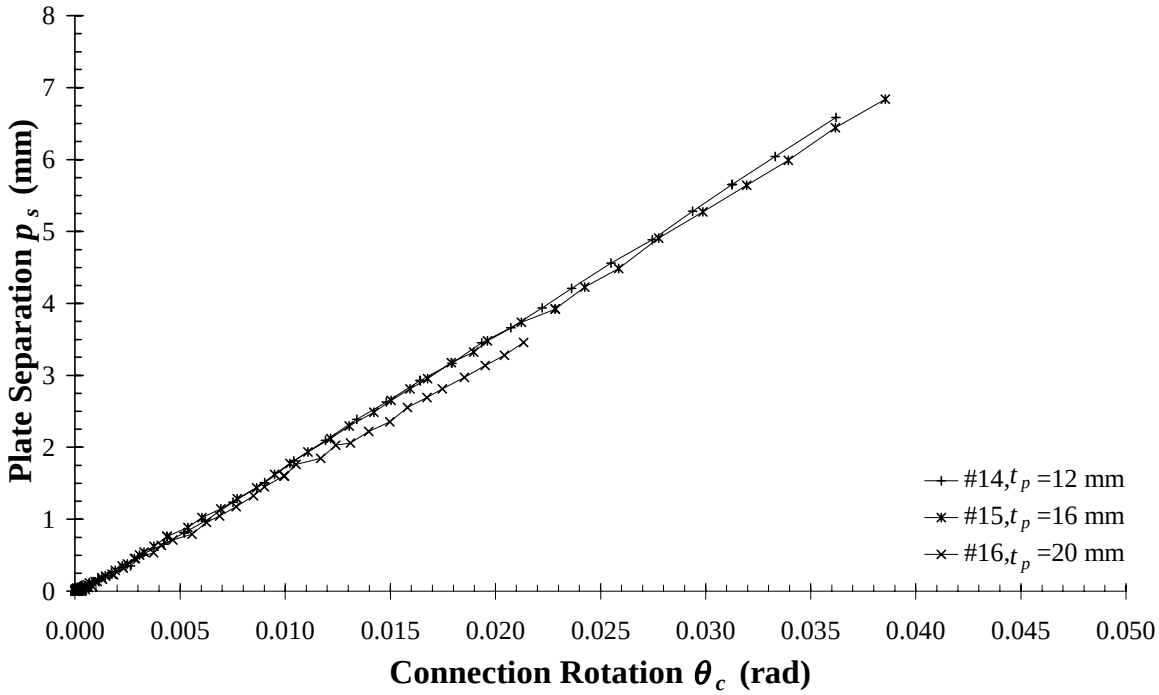

FIG A33: CONNECTION ROTATION VS. PLATE SEPARATION for Type B Connections - Rectangular Hollow Sections, W_p=160mm

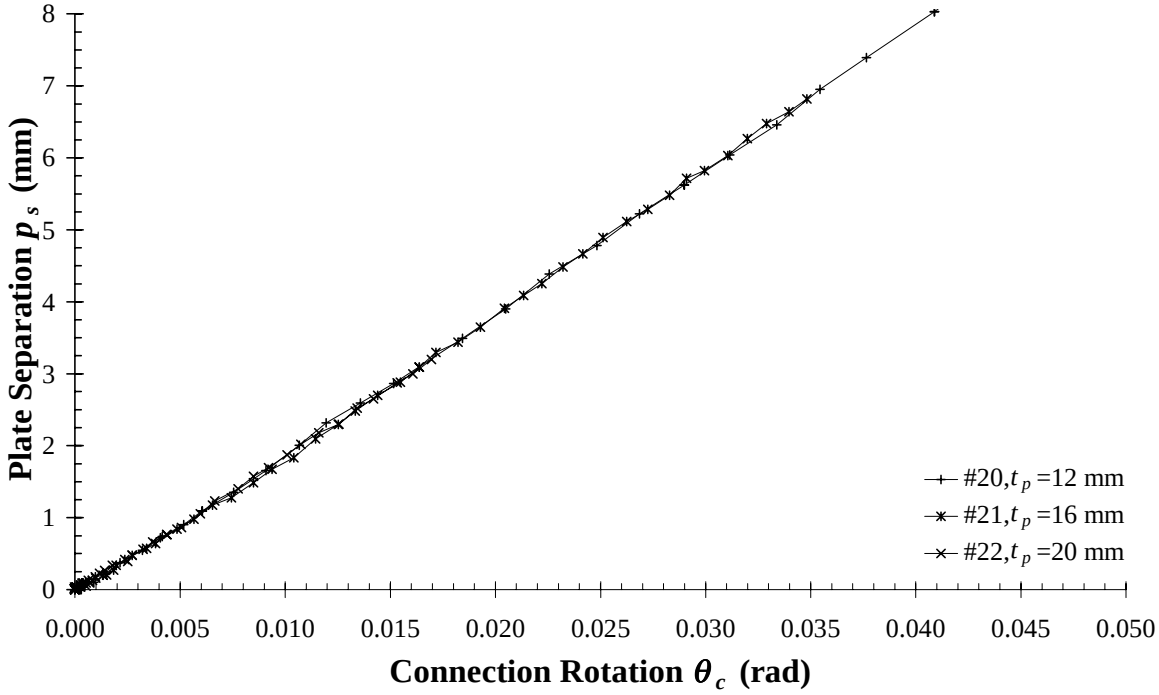

FIG A34: CONNECTION ROTATION VS. PLATE SEPARATION for Type B Connections - Rectangular Hollow Sections, W_p=230mm

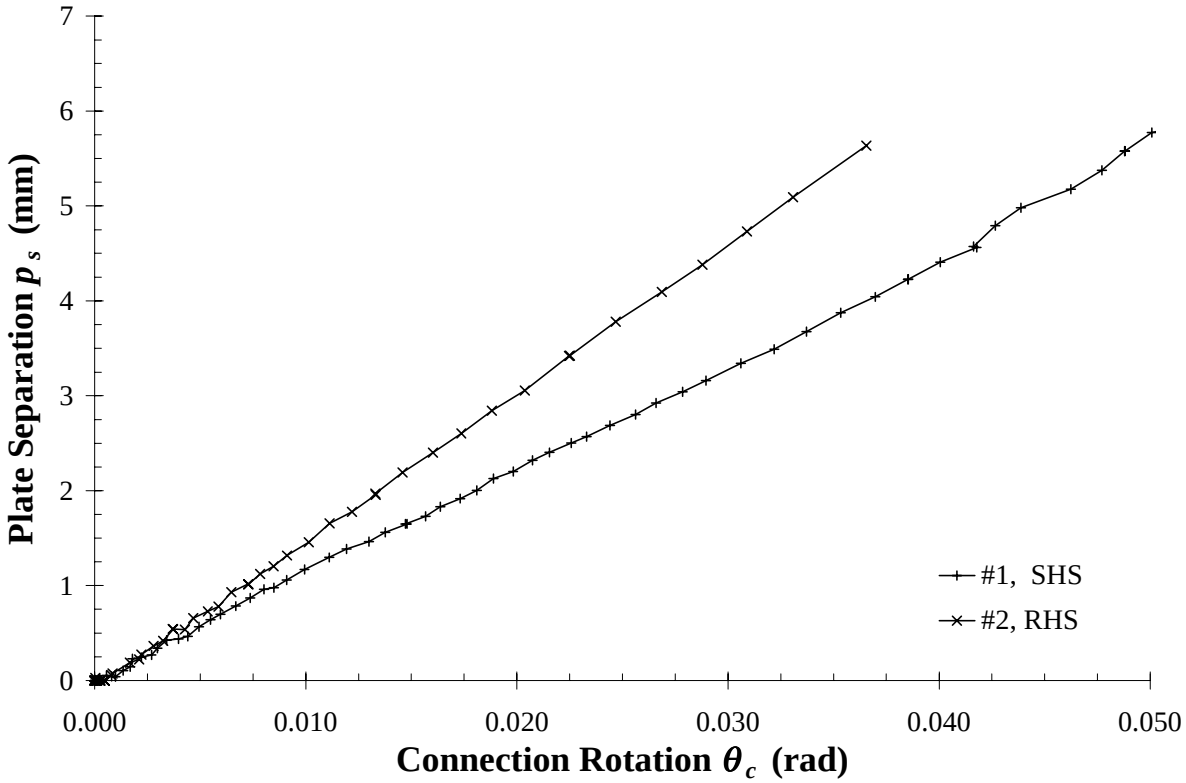

FIG A35: CONNECTION ROTATION VS. PLATE SEPARATION for Type A Connections - t_p=16 mm

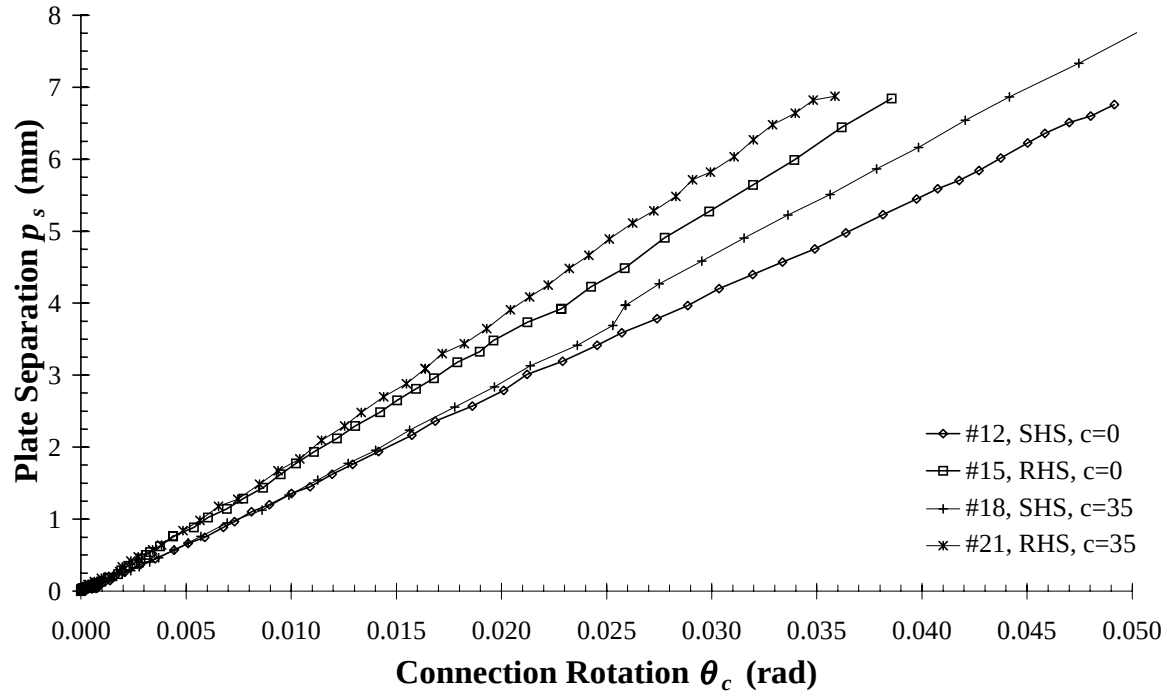

FIG A36: CONNECTION ROTATION VS. PLATE SEPARATION for Type B Connections - t_p=16 mm

APPENDIX B - *Welding Procedure*

Appendix C - *Linear Correlation Analysis*

The linear correlation coefficient (r), based on a series of n points (x_i, y_i) can be calculate using (Freund 1988):

$$r = \frac{S_{xy}}{\sqrt{S_{xx} \cdot S_{yy}}}$$

where $S_{xx} = \sum x_i^2 - \frac{1}{n}\left(\sum x_i\right)^2$,

$$S_{yy} = \sum y_i^2 - \frac{1}{n}\left(\sum y_i\right)^2,$$

$$S_{xy} = \sum x_i y_i - \frac{1}{n}\left(\sum x_i\right)\left(\sum y_i\right)$$

The result of $|r| = 1$ is indicative of a perfect linear fit, while a result of $|r| = 0$ indicates no linear correlation. Using a 5% level of acceptance it can be said that if $|r| < 0.975$ there is no linear correlation.

In the present application using $x_i = (\theta_c)_i$ and $y_i = (p_s)_i$ the correlation coefficients (r) have been calculated for each test and are shown in Table C1, where i represents a particular experimental reading during a test comprising of n such points. For all tests, the correlation coefficient is greater than 0.975, thus confirming a linear relationship between connection rotation and plate separation. This relationship is shown graphically by the plots of θ_s *vs.* p_s for each tests in Appendix A (Figures A29-A36).

The relationship between plate separation (p_s) and connection rotation (θ_c) can thus be expressed as

$$p_s = m \cdot \theta_c$$

The constant (m) is tabulated in Table C1 and has been derived using the method of least squares.

The constant m is primarily dependant on the depth of the section (d), with the dimensions of the end plate also having a significant effect (see Figure A36).

Table C1 -Correlation Analysis Results

Test Number	Correlation Coefficient	Coefficient m
1	0.999	109.0
2	1.000	150.9
3	1.000	111.0
4	0.995	110.3
5	1.000	169.8
6	0.998	153.0
7	0.992	93.1
8	1.000	126.8
9	0.999	154.0
10	1.000	157.8
11	1.000	142.4
12	1.000	137.6
13	1.000	131.0
14	1.000	180.0
15	1.000	175.7
16	1.000	159.9
17	1.000	151.6
18	1.000	153.7
19	1.000	143.8
20	0.996	192.1
21	1.000	192.9
22	1.000	186.8
23	0.996	147.5
24	1.000	145.5
25	1.000	188.1
26	1.000	196.1